Spring 2019

Measuring and Modeling Bare Desert Wind Erosion From Steppe Grassland of Northern China as Affected By Soil Moisture and Climate

Nicholas Morgan Potter
Old Dominion University, nickpotter221@gmail.com

MEASURING AND MODELING BARE DESERT WIND EROSION FROM STEPPE GRASSLAND OF NORTHERN CHINA AS AFFECTED BY SOIL MOISTURE AND CLIMATE

by

Nicholas Morgan Potter
B.S. May 2018, Old Dominion University

A Thesis Submitted to the Faculty of
Old Dominion University in Partial Fulfillment of the
Requirements for the Degree of
MASTER OF SCIENCE
CIVIL ENGINEERING
OLD DOMINION UNIVERSITY
May 2019

Approved by:

Xixi Wang (Director)

Gary Schafran (Member)

Yewei Zheng (Member)

ABSTRACT

MEASURING AND MODELING BARE DESERT WIND EROSION FROM STEPPE GRASSLAND OF CHINA AS AFFECTED BY SOIL MOISTURE AND CLIMATE

Nicholas Morgan Potter

Old Dominion University, 2019

Director: Dr. Xixi Wang

Soil erosion by wind has been found to be negatively related to soil water content, as evidenced by that for a given area, such a soil erosion can be much less in a wet than a dry year. However, few studies have examined the functional relationship between wind erosion and soil moisture, primarily due to lack of field measured data. The objectives of this study were to: 1) measure wind erosion in field using a portable wind tunnel devised and made by the author; 2) use the measured data to calibrate/validate a wind erosion model previously developed by the author; 3) model the potential effects of climate change via changes in moisture and wind speed. The study was conducted in the steppe grassland within the Balagaer river watershed located in north China. As part of a larger project funded by the National Science Foundation, this study focused on soil conditions with a minimal vegetation coverage to understand the functional relationship between wind erosion, soil moisture, and climate. These conditions are similar with those during winter and spring and/or when the grassland degrades and ultimately becomes a desert. Field samples were analyzed in a laboratory to determine the soil characteristics (e.g., moisture content, texture, hydraulic conductivity, and organic content).

ACKNOWLEDGEMENTS

This study is part of a project (#1654957) funded by the National Science Foundation (NSF) International Research Experience for Students (IRES) program. Students from Old Dominion University (ODU), Norfolk, VA, USA, Inner Mongolia University (IMU), Hohhot, Inner Mongolia, China, and Inner Mongolia Agricultural University (IMAU), Hohhot, Inner Mongolia, China, all contributed to the project. In addition, the appreciations are also extended to the four Chinese mentoring professors from IMAU and IMU, including Dr. Ruizhong Gao, Dr. Ruihong Yu, Dr. Yanyun Luo, and Dr. Fengling Li. Further, it might be impossible to complete my degree without the support and patience of my highly-respected parents, Marion Potter and Carol Potter.

NOMENCLATURE

q_a	Wind erosion modulus, g m^{-2} s^{-1}
C_a	Soil-specific coefficient of wind erosion when the surface soil is bare and dry, g m^{-5} s^2
τ_*	Effective wind shear stress, N m^{-2}
τ_{*c}	Threshold wind shear stress, N m^{-2}
u	Wind speed, m s^{-1}
u_*	Friction shear velocity at the ground surface, m s^{-1}
u_*'	Friction shear velocity at the zero-plane displacement height, m s^{-1}
$u_{*\psi}$	Threshold friction shear velocity when the surface soil is bare and dry, m s^{-1}
$u_{*\theta}$	Threshold friction shear velocity when the surface soil is bare but moist, m s^{-1}
$u_{*\theta\lambda}$	Threshold friction shear velocity when the surface soil is vegetated and moist, m s^{-1}
g	gravitational acceleration, m s^{-2}
f_w	Dimensionless coefficient that reflects effects of surface soil moisture
P_{clay}	Clay content in the soil, %
θ	Surface soil volumetric water content (i.e., moisture)
ω	Surface soil mass water content
ω’	Threshold water content
ρ_s	Soil particle density, kg m^{-3}
ρ_{air}	Density of air, kg m^{-3}
ρ_w	Density of water, kg m^{-3}
κ	von Karman constant (= 0.41)
d	Zero-plane displacement height, m
d_s	Diameter of surface soil particle, m
a_1	First coefficient related to threshold shear stress, dimensionless
a_2	Second coefficient related to threshold shear stress, dimensionless
z_0	Surface roughness length, m
z	Height of wind speed, m

h	Average vegetation height, m
λ	Vegetation roughness density
e	Soil void ratio
ER	Erosion rate (mm yr^{-1})
A	Area of interest (m^2)

TABLE OF CONTENTS

Page

ABSTRACT ii

ACKNOWLEDGEMENTS iii

NOMENCLATURE iv

LIST OF TABLES viii

LIST OF FIGURES ix

LIST OF EQUATIONS xi

CHAPTER

1. INTRODUCTION 1

    1.1 Background 1

    1.2 Literature Review 2

    1.3 Objectives 7

2. CLIMATE AND PHYSIOGRAPHY 8

    2.1 The Balagaer River Watershed 8

    2.2 The Specific Sites 11

3. METHODS AND MATERIALS 14

    3.1 Rationale of Wind Tunnel Development 14

    3.2 The Portable Wind Tunnel System 15

    3.3 Data Collection 20

3.4 Data from Previous Study 21

3.5 Results and Discussion 22

4. MODELING 29

4.1 Description of IAFP 29

4.2 Parameterization of the IAFP Model 32

4.3 Hypothetical Scenarios and Predicted Erosion Rates 33

4.4 Discussion 38

5. CONCLUSIONS 41

6. RECOMMENDATIONS FOR FUTURE RESEARCH 42

APPENDIX: STATISTICS OF THE AVERAGE DAILY WIND SPEEDS FROM 1955 TO 2010 43

REFERENCES 44

CURRICULUM VITA 48

LIST OF TABLES

Table Page

2.1. Locations and initial conditions of the specific sites 12

3.1 The field test data 19

LIST OF FIGURES

Figure Page

2.1. Location and boundary of the Balagaer River watershed, superposed by the World Food and Agriculture Organization (FAO, 2008) soil associations 8

2.2. Whisker plots showing variations in monthly wind speeds from 2006 to 2010.....10

2.3. Histogram of the historical wind speeds.....10

2.4. Typical site conditions.....11

3.1. Pictures of the: (a) downwind view of the Portable Wind Tunnel (PWT) system; and (b) top view of its contraction section.....16

3.2. Frontal view of the slot sampler.....16

3.3. Pictures of the: (a) collection container; (b) filter scheme.....18

3.4. Box and whisker plot of the measured erosion rate, and b) histogram of the simulated wind speeds.....23

3.5. Erosion vs wind speed. 23

3.6. Erosion vs. water content.....24

3.7. Velocity profile at the front port.....25

3.8. Velocity profile at the middle port.....25

3.9. Velocity profile at the back port 26

4.1. The modeled versus measured soil erosion rates by the portable wind tunnel (PWT).....33

4.2. The predicted erosion rate versus hypothetical soil water content ($u = 4.8$ m s^{-1}). 34

4.3. The predicted erosion rate versus hypothetical wind speed for various water contents.....35

4.4. The predicted erosion rate versus hypothetical particle density ($u = 4.8$ m s^{-1}). 36

4.5. Plot showing the: (a) annual average daily soil moisture and wind speed; and(b) annual average daily water content and wind speed. The record period is from 1 January 2006 to 31 December 2010. The wind speed (u2) was measured at 2 m above the ground surface. 37

4.6. The predicted historical daily erosion rates for the Balagaer River watershed. 38

LIST OF EQUATIONS

Equation Page

(1) Wind erosion module 6, 29

(2) Threshold shear stress 30

(3) Threshold surface friction shear velocity 30

(4) Dimensionless coefficient 30

(5) Threshold water content 30

(6) Soil moisture 30

(7) Bulk density (soil moisture) 30

(8) Bulk density (soil water content) 30

(9) Threshold friction shear velocity when the surface soil is bare and dry 31

(10) Effective shear stress 31

(11) Friction shear velocity at the ground surface 31

(12) Surface roughness length 31

(13) Soil erosion rate 32

CHAPTER 1:
INTRODUCTION

1.1 Background

Over the years, land degradation and climate change have been of most concern for future development and sustainability. In this regard, the target area of this study was in the Eurasian steppe grassland region where there is an enormous industry for livestock production. Thus, the impacts of transportation, overgrazing, cultivation, and climate change are vital modes that need to be managed to continue the high productivity of this grassland. Overgrazing occurs when livestock consumption is more than vegetation production and can consequently cause stunned vegetation growth and exposed soils. In the case of climate change, there is an increase in aridity and a decrease in soil moisture; this is especially true for the early spring conditions when there is hardly any vegetation growth.

During spring, there are frequent dust storms that can be heightened from the excess of bare soil, causing not only a health problem for people but also fertility loss as the topsoil is detached. As a result, the vegetation coverage may be lost and fail to mitigate further erosion of topsoil. The above factors of soil erosion can be amplified by urbanization, land use change, and other human activities (e.g., tourism). However, there are few data and tests regarding how soil moisture and wind speed interactively affect topsoil erosion. This study intended to fill such an information gap and thus will advance our scientific understanding of the thresholds that may trigger irreversible land degradation, making it possible to develop practical measures to sustain the vulnerable steppe ecosystem. The test bed of this study was the 5350 km^2 Balagaer River watershed, located in northeast Inner Mongolia Autonomous Region of China.

1.2 Literature Review

Wind erosion is not a new process, as it is a naturally occurring phenomenon in which soil particles are displaced from one location to another. Normally the erosion impacts are low due to the time in which they occur however due to the anthropogenic disturbances the erosion has been accelerating in frequency (Meng *et al.,* 2018). As an effect of human activities, in China 90% of grasslands have been suffering from degradation (Yan *et al.,* 2010). China is a vast country with 50% of its land coverage considered to be susceptible to wind erosion (Meng *et al.,* 2018). Land cover such as vegetation cover is crucial for mitigating the acceleration of erosion because the vegetation not only slows the wind speed down to zero-flux height but also traps the eroded particles (Nyamtseren *et al.,* 2016; Wolfe and Nickling, 1993; and Musick and Gillette 1990). Likewise, as there is more pressure to increase livestock there is a decrease in vegetation which lowers the zero-flux height (Li *et al.,* 2005).

Climate change has been facilitated by the extensive human activities, and the Inner Mongolian Steppe Grasslands are no exception as it is highly susceptible to climate change (Shao *et al.*, 2017; Wang *et al.*, 2014a; National Intelligence Council, 2009; Wu and Loucks, 1992). The air temperature had been predicted to increase at a rate of 0.35 C° per ten years, increasing the potential for wind erosion due to soil moisture reduction (Shao *et al.,* 2017). Previous studies (e.g., National Intelligence Council, 2009) revealed that the warming in winter and spring in northern China had induced 29% of the total dust emissions in Asia (National Intelligence Council, 2009). In the recent decades, the impacts of climate change on soil erosion are well known and have been studied extensively (Guo *et al.*, 2017; Shao *et al.*, 2017; Wang *et al.*, 2014a; Chen *et al.*, 1996).

Meng *et al.,* (2018) conducted wind speed erosion measurements using an *in-situ* wind

tunnel to find the threshold vegetation cover to prevent erosion at different wind speeds, as well as studying the relationship of wind erosion and soil. The study location was in the desert steppe of Inner Mongolia, China and this location is said to obtain the source of such eroded sand to produce a sandstorm in Beijing (Meng *et al.,* 2018). Historical data shows the annual average wind speed at 10 m above the ground was 4.5 m s^{-1} and seasonal wind speeds in the spring being 5 to 18 m s^{-1}.

The wind tunnel that was used was a mobile wind tunnel with dimensions of 1.0 m wide, 7.2 m long, and 1.2 m height (Meng *et al.,* 2018). Wind erosion tests were conducted with a varying wind speed between 2 to 20 m s^{-1}, with incremental vegetation, at an average of ten-minute intervals, and soil moisture varying from 3.5% to 9.5%. Wind speed was measured at 30 cm from the ground using a pitot-tube device. Furthermore, the previous parameters were tested under specific experimental conditions to better understand the parameter individually related to erosion (i.e., varying one parameter per test sequence). Erosion samples were collected at different vertical heights from 2 to 70 cm with separator sand sampler from horizontal displaced sand mass (Meng *et al.,* 2018).

Note that the experimental test was conducted during March to July as after July the windy season stops, and the rainy season starts. Moreover, the concentration of wind erosion in terms of mass flux was concentrated closer to the ground from 0 to 30 cm with vegetation cover at 15%. Regression analysis was performed to model wind erosion trends of vegetation cover, moisture, and wind speed with changes in height, correspondingly the regression equations were power series. All of the distribution decreased in sand mass flux as height increased. The mobile wind tunnel test concluded that the significant factors from are the following in "…descending order: wind speed, vegetation coverage, and soil moisture" (Meng *et al.,* 2018).

A study, conducted by Chen *et al.* (1996) to measure and predict soil erosion from the Loess Plateau in north China, showed how soil moisture and wind speed could interactively affect erosion. The study was performed using a laboratory wind tunnel with undisturbed surface soil sample blocks (100 cm long, 30 cm wide, and 25 cm high) taken from the field. The erosion tests were conducted using three soil samples, which are classified as loessal loam sandy, loamy sand, and sandy loam, respectively. For each of the samples, the tests were conducted at various soil moisture levels and wind speeds. As expected, the study indicated that the loessal sandy loam sample is much more erodible than the other two samples because of its loose structure.

The wind tunnel used by Chen *et al.* (1996) has a working section of 16 m long, 1 m wide, and 0.6 m high. The soil water contents were measured using the overdried method with sampling before and after testing. The duration for each test varied from 2 to 15 minutes; wind speeds were measured using a pitot tube at a constant height of 30 cm from the soil surface. For a given test, the number of eroded soils was measured as the weight loss of the sample block via an electric balance and verified by the number of soils collected at the end of the working section. The tests indicated a threshold water content of 4 to 6 % irrespective of the soil classifications, below which the detachment and movement of soil particles incepted.

Strong *et al.* (2016) devised a micro wind tunnel (MWT) for on-site erosion measurement. The wind tunnel was made small enough to be portable to accomplish in-situ testing and functionally simulate historical wind speeds. A field testing of the MWT was performed in the semiarid landscape of Longreach, Queensland, Australia, with the purpose of studying livestock pressure on erodible soils. The MWT was deployed in various locations with high to low livestock pressures and clay and sandy loam soils.

The MWT by Strong *et al.* (2016) consists of a contraction section, a transition section, a

working section, a sediment trap, an exhaust section, a wind velocity regulator, a 280-mm-diameter axial fan, and several wind speed sensors. Three keyholes were drilled in respective distance from the front of the working section at 100, 450, and 900 mm, respectively. These holes were used to measure wind speeds using a static-pitot tube at three different heights. Because of the small height of the MWT, the pressure ports were used to measure the pressure gradients, which in turn were used to calculate the wind speed and shear stress at the soil surface instead of using a velocity profile. The winds speeds ranged from 5 to 18 m s^{-1} with high reproducibility. The MWT proved to be applicable for wind erosion simulations in fields with a bare open space constrained by grass clumps.

Over the years, wind and water erosion has been evaluated as separate entities due the nature of occurrence as wind erosion occurs during typically dry conditions were as water erosion occur during higher soil water contents. However, due to fluctuations in water content both erosion processes can occur in a relatively temporal frequency. So, the theory that both wind and water erosion have a significant trigger factor to produce the maximum erosion was proposed by Ravi *et al.,* 2010. The idea states that when the soil moisture increases from zero wind is the controlling erosion process, then there is a zone where the wind and water share contribution to total erosion, and finally the moisture content increase the threshold where no wind erosion contributes and is totally water erosion controlled (Ravi *et al.,* 2010). In the study of the "interactions among hydrologic–aeolian erosion" there were no quantitative results that describe the threshold of factor that control erosion (Ravi *et al.,* 2010).

Wang *et al.* (2014b) developed an integrated aeolian and fluvial prediction (IAFP) model in terms of the physical mechanisms of these two types of erosion processes. The IAFP model was tested in the Balagaer River watershed. The model's unique feature was to predict wind and

water erosions as a whole rather than separately. In the convention, these two types of erosions have been treated separately although they are physically connected. The fundamental dynamics of soil erosion is that the shear stress induced by wind detaches some soil particles from their adherent particles. The minimum shear stress required to detach the soil particles, which is defined as the threshold wind shear stress, depends on soil type, texture, structure, and moisture as well as physiological characteristics of the covering vegetation species (e.g., leaf area and height). When the wind speed reaches a magnitude to induce effective shear stress above the threshold, the difference between the shear stress and the threshold is positively related to soil erosion. The wind speed corresponding to the threshold shear stress is called the threshold wind speed. When the actual wind speed is smaller than the threshold wind speed, no erosion will occur. From now on, unless specified otherwise, erosion is defined as the movement of soil particles in suspension, saltation, or creep. The IAFP calculates wind soil erosion as:

$$q_a = C_a \left(\frac{\tau_* - \tau_{*c}}{\rho_{air}}\right)^{\frac{3}{2}} \quad (1)$$

where q_a is the wind erosion modulus (kg m^{-2} s^{-1}); C_a is a soil-specific coefficient when the surface soil is bare and dry; τ_* is the effective wind shear stress (N m^{-2}); τ_{*c} is the threshold wind shear stress (N m^{-2}); ρ_{air} is the density of air (kg m^{-3}).

Wang *et al.* (2014b) estimated C_a by two steps. Firstly, the slope by linearly regressing the literature values of q_a over those of $\left(\frac{\tau_* - \tau_{*c}}{\rho_{air}}\right)^{\frac{3}{2}}$ was determined. Secondly, the determined slope was divided by an area-influence factor to derive the C_a value for the watershed of interest. The area-influence factor, calculated as the square root of the ratio of the watershed area to the soil sample erosive surface area, was used to account for the soil particle suspension and deposition processes within the watershed. In our subject knowledge, for a given wind tunnel test, the area-

influence factor should be larger for a larger than a smaller watershed. Because site-specific test data were unavailable and not used, the C_a value reported by Wang *et al.* (2014b) was revisited in terms of the data collected in this study.

1.3 Objectives and Goals

The overarching goal of this study was to advance our understanding of wind erosion as affected by human activity and climate change. The specific objectives were to: 1) devise and use a portable wind tunnel to measure in situ soil erosion; 2) use the measured data to calibrate and validate the wind erosion component of the IAFP model; and 3) use the calibrated model to predict the potential effects of soil moisture and wind speed changes on soil erosion.

CHAPTER 2
CLIMATE AND PHYSIOGRAPHY

2.1 Balagaer River Watershed

The location of interest for the study was Balagaer River Watershed, which is positioned in the Inner Mongolian Autonomous Region of China shown in (Figure 2.1). Furthermore, the watershed is comprised of 5350 km^2 with elevations varying from 870 m to 1055 m above sea level (Wang *et al*. 2014b). The soil profile consists of mainly two sections from the ground surface down to 30 cm of loamy sand and 30 to 100 cm of predominantly sandy soil. The soil surface consisted of sand particle size of 0.05 to 2 mm in diameter and silt particle size that of 0.002 to 0.05 mm in diameter with a primary soil particle diameter of 0.125 to 0.25 mm, with a mean of 0.15 mm (Wang *et al.* 2014b). Furthermore, soil clay percent is less than 30%.

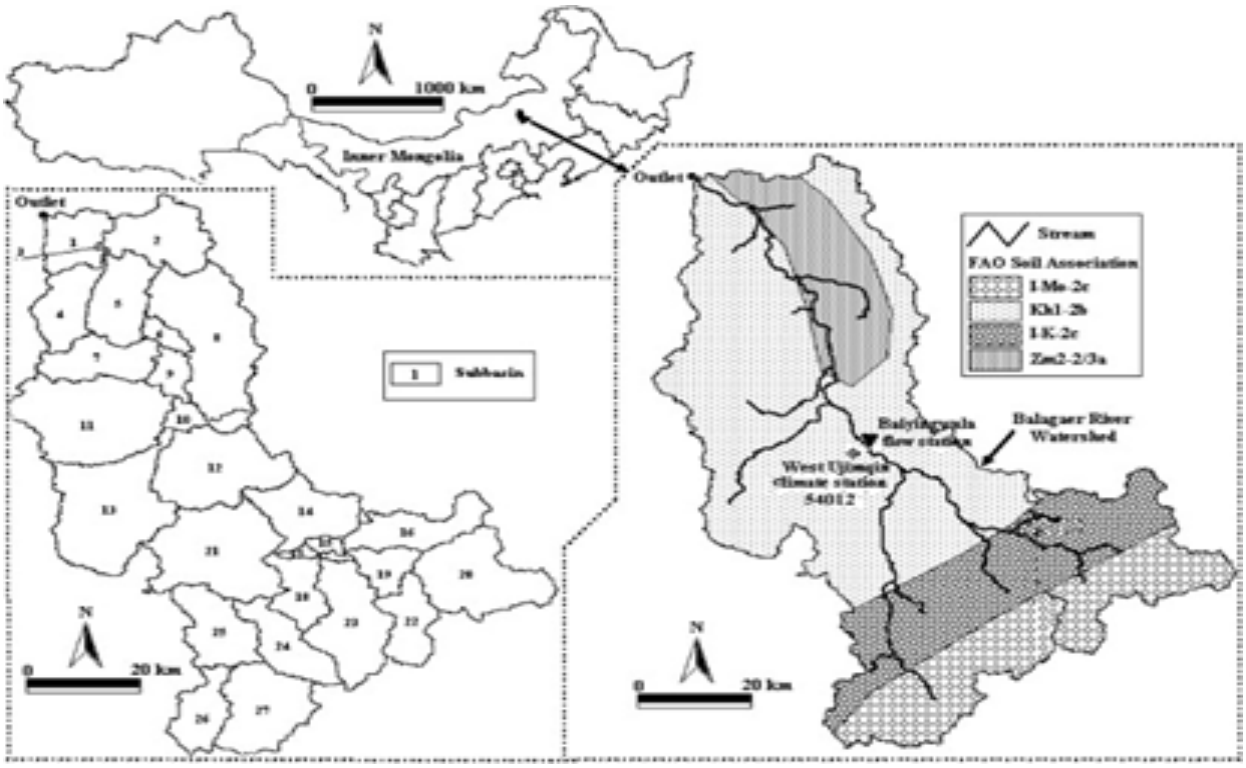

Figure 2.1. Location and boundary of the Balagaer River watershed, superposed by the World Food and Agriculture Organization (FAO, 2008) soil associations.

Weather data has been collected from 1955 to 2010 from the West Ujimqin Climate station 54012 (117°36′E, 44°35′N, (Figure 2.1)) on the specific site which includes, but limited to, wind speed, moisture content, and air temperature Wang *et al.* (2014). Soil moisture ranged from a wilting point (θ_{ψ}) of 0.012, a field capacity of (θ_{fc}) 0.09 for optimum plant growth and a saturation point (θ_{sat}) of 0.26. The region is classified as semiarid with average precipitation of 312 mm per year (Wang *et al.* (2014b).

Statistical box and whisker plots were generated from yearly frequency wind speeds from 1955 to 2010 to get trends in wind speed; thus, there was a slight decrease in wind speed, with the last five years having increased wind speeds (Figure 2.2). So, no significant trend up or down can be determined, as shown in Appendix A. The annual daily mean wind speed for the last five years of wind record from 2006 to 2010 was 4.2 m s^{-1}. Further, seasonal plots show that there was a biannual fluctuation in wind speeds exhibiting relatively elevated wind speeds in winter and spring compared to summer and fall (Figure 2.3). The histogram of daily wind speeds from 1955 to 2010 (Figure 2.2) showed that there was a central tendency of wind speeds to be observed and arithmetically calculated to be 3.78 m s^{-1}. Moreover, the land use is predominantly husbandry livestock with others being agriculture and developing industry.

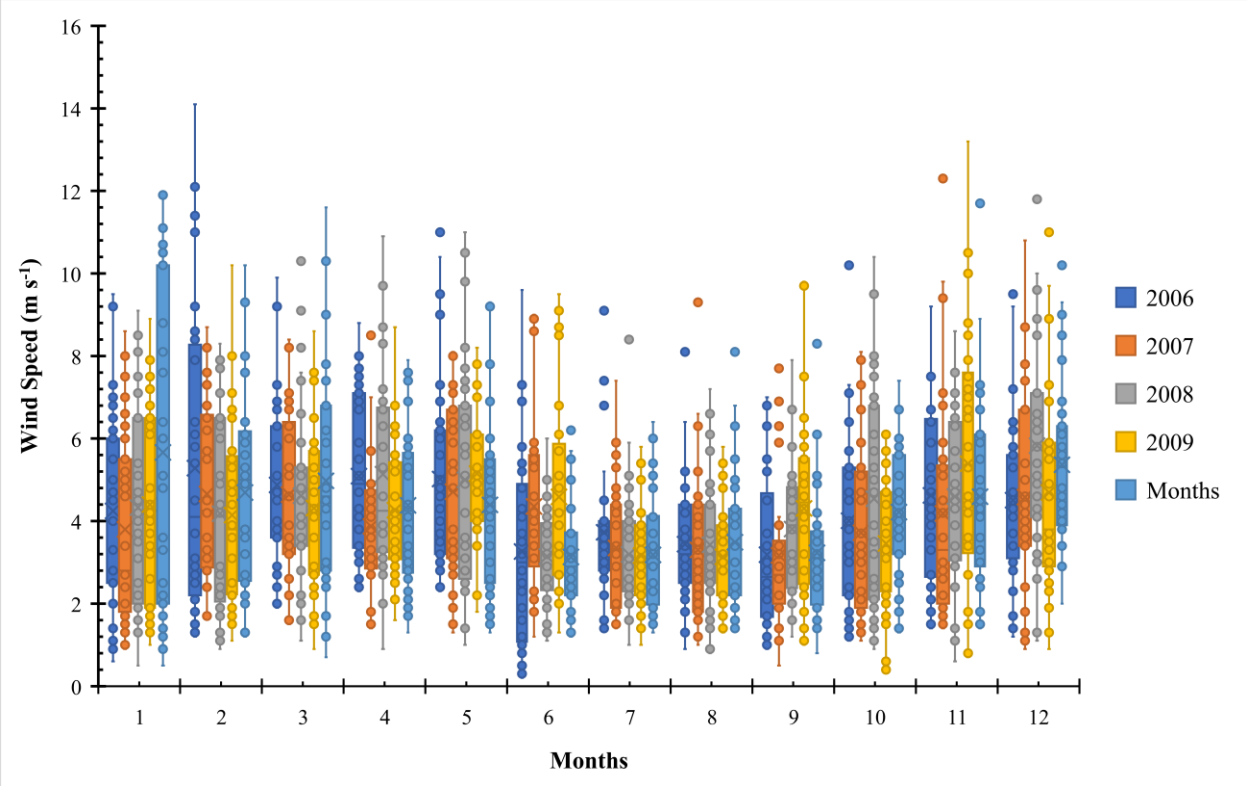

Figure 2.2. Whisker plots showing variations in monthly wind speeds from 2006 to 2010.

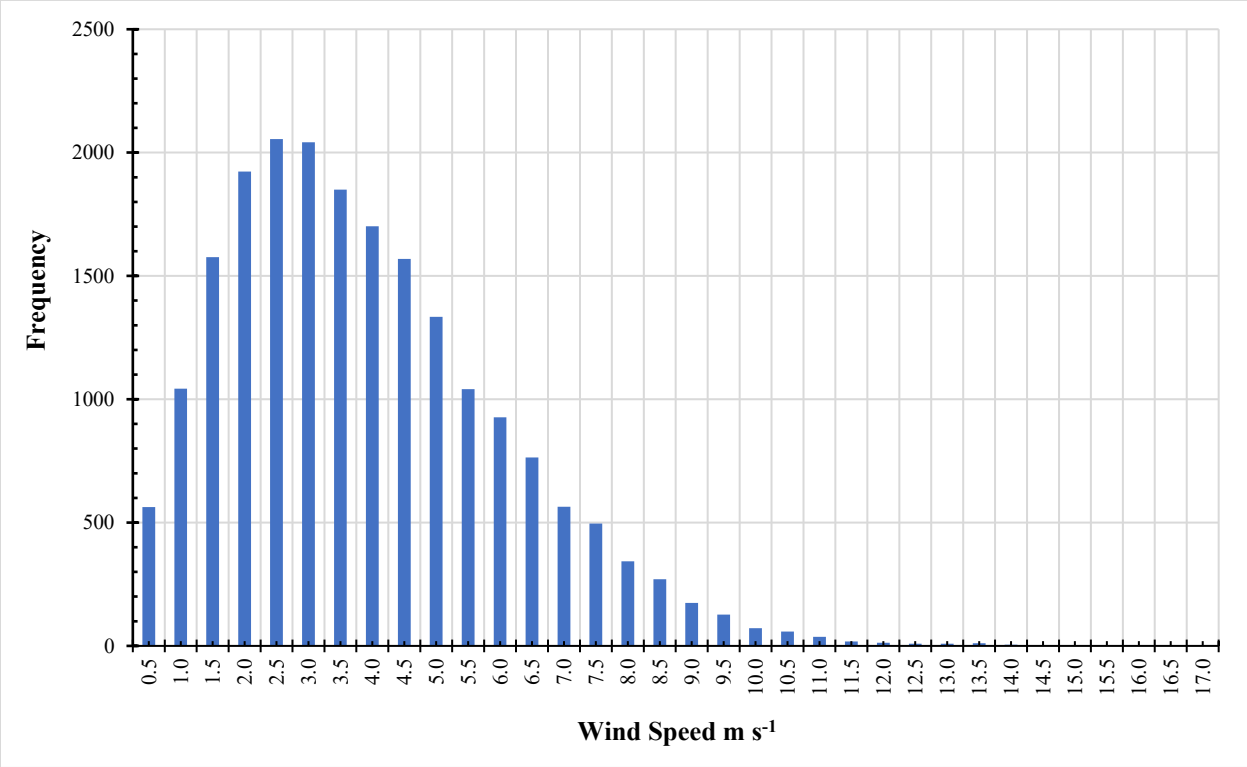

Figure 2.3. Histogram of the historical wind speeds.

2.2 The Specific Sites

Site selections were captured within the boundary of the land owner's property. The decisions on where to perform wind simulations are characterized by needs of the wind erosion modeling parameters. Thus, the sites were chosen that exemplified one with loose in natural but were not excessively disturbed (i.e., rain or animal packed). Each site was selected based on the following characteristics: bare, dry, and with insignificant debris. Typically, observed site conditions can be seen in Figure 2.4. Sites were found with the best uniformity of soil surface in between large clumps of grass; in these locations, there were minimal disturbances. Away from the grass clumps there was more uniform low-lying grasses but had a relatively large density of plants (e.g., not bare). The soil conditions were observed to be visually equivalent in texture, soil particle size (not excessive sand from previous erosion of smaller particles), and dry in moisture. The sites chosen had little to no slope with an average of 1.2 percent slope. The locations of the 31 sites are shown in Table 2.1.

Figure 2.4. Typical site conditions.

Table 2.1. Locations and initial conditions of the specific sites.

TEST NUMBER	DATE	LONGITUDE (DEGREE)	LATITUDE (DEGREE)	SLOPE (%)	DIRECTION (DEGREE)	SOIL MOISTURE (θ)	SOIL CONDITIONS
1.1	6/25/18	44.3319331	117.866602	1		0.071	Bare/Dry sandy soil
1.2	6/25/18	44.3319331	117.866602	1		0.071	Bare/Dry sandy soil
2.1	6/25/18	44.331953	117.866883	1.9	245 E TO W	0.046	Bare/Dry sandy soil
3.1	6/25/18	44.331933	117.866847		162 N TO S	0.031	Bare/Dry sandy soil
4.1	6/29/18	44.331977	117.865008	0	2.1 S TO N	0.036	Bare/Dry sandy soil
5.1	6/29/18	44.332063	117.86504	0.7	289 E TO W	0.033	Bare/Dry sandy soil
6.1	6/29/18	44.332059	117.865066	0.5	258 E TO W	0.033	Bare/Dry sandy soil
7.1	6/29/18	44.332059	117.865066	0.4	119 NW TO SE	0.036	Bare/Dry sandy soil
8.1	7/2/18	44.331908	117.865528	0.3	209 NE TO SW	0.02	Bare/Dry sandy soil
9.1	7/2/18	44.331908	117.865528	0.6	193 NE TO SW	0.027	Bare/Dry sandy soil
10.1	7/2/18	44.331953	117.866883	1.3	335 SE TO NW	0.03	Bare/Dry sandy soil
11.1	7/10/18	44.332223	117.866401	0	56 SW TO NE	0.035	Bare/Dry sandy soil
12.1	7/10/18	44.332175	117.866667	0	359 S TO N	0.04	Bare/Dry sandy soil
13.1	7/10/18	44.332163	117.866407	1	332 SE TO NW	0.035	Bare/Dry sandy soil
14.1	7/10/18	44.332148	117.866353	1.9	277 E TO W	0.036	Bare/Dry sandy soil
15.1	7/14/18	44.331136	117.867902	1.6	20 SW TO NE	0.04	Bare/Dry sandy soil
16.1	7/14/18	44.331331	117.867867	0.5	84 W TO E	0.035	Bare/Dry sandy soil
17.1	7/14/18	44.331332	117.867874	0.6	75 W TO E	0.035	Bare/Dry sandy soil
18.1	7/14/18	44.331333	117.86788	0.9	82 W TO E	0.042	Bare/Dry sandy soil
19.1	7/15/18	44.331343	117.867852	3.4	340 S TO N	0.06	Bare/Dry sandy soil
20.1	7/15/18	44.331323	117.867883	3.5	342 S TO N	0.06	Bare/Dry sandy soil
21.1	7/15/18	44.331321	117.867827	2.9	342 S TO N	0.06	Bare/Dry sandy soil
22.1	7/15/18	44.331319	117.86783	4	337 S TO N	0.05	Bare/Dry sandy soil
23.1	7/19/18	44.331335	117.867869	0	54 SW TO WE	0.052	Bare/Dry sandy soil

24.1	7/19/18	44.331342	117.867874	1	69 W TO E	0.042	Bare/Dry sandy soil
25.1	7/19/18	44.331326	117.867852	1.1	81 W TO E	0.071	Bare/Dry sandy soil
26.1	7/19/18	44.331345	117.867871	1.5	72 W TO E	0.083	Bare/Dry sandy soil
27.1	7/28/18	44.331323	117.867887	1.2	31 SW TO NE	0.094	Bare/Dry sandy soil
28.1	7/28/18	44.331331	117.867893	0.8	22 SW TO NE	0.068	Bare/Dry sandy soil
29.1	7/28/18	44.331333	117.867895	0.9	37 SW TO NE	0.066	Bare/Dry sandy soil
30.1	7/28/18	44.331352	117.867856	1.7	57 SW TO NE	0.052	Bare/Dry sandy soil

CHAPTER 3:
METHODS AND MATERIALS

3.1. Rationale of Wind Tunnel Development

A portable wind tunnel (PWT) is the best suitable device to simulate wind in the field due to the condition of the study Steppe Grassland because of the following factors: transportation, footprint, deployment, and assembling. In the development of the PWT, the objective was to simulate wind speeds that were historically equivalent, thus creating the similar conditions at which erosion could be measured. Since the grassland has many different types of terrain, slopes and ground cover, it is not viable to block sample or recreate the field conditions in the laboratory. With the PWT, the consecutive tests could be simulated with little spatial repositioning, i.e., after one test was concluded, then the PWT was moved to a new location to minimize the effects of limiting erosion. Special considerations were made so that the instrument could be easily transported by a typical vehicle and conversely be carried by person power; firstly, to be small enough to fit into a vehicle, and secondly, to minimize the impacts on the grassland. Logistics of the transportation of the wind tunnel had to be kept in mind as the available vehicle space was limited, especially regarding the generator and length of tunnel sections. The size if the PWT needed to be where the working section of the wind tunnel could be generalized as homogenous and be able to fit in between grass clumps or obstructions. Furthermore, the assembly of the PWT needs to be that it could be constructed by the author without extraordinary skills while with the materials that could be found in the developing area.

There have been previous uses of a portable field wind tunnel such as the micro wind tunnel previously mentioned by Strong *et al.,* (2016) with similar aspects in the development relative conditions of the testing. Their micro wind tunnel was designed for a semiarid climate

which is like the condition of this study (Strong *et al.*, 2016). To accomplish usable wind data, the PWT needed to produce laminar flow or smooth wind patterns, variable wind speeds, sediment collection without wind restriction, and access to reading different heights of the wind velocity profile.

3.2 The Portable Wind Tunnel System

With in-situ field testing in mind, the PWT system (Figure 3.1) consists of a contraction section, a transition section, working section, primary suction fan, slot sampler, collection container, collection suction fan, and power source. Additional items were the digital wire anemometer, moisture meter, steel plates, duct tape, and sample containers. The contraction section enabled smooth wind flow (Figure 3.2) and was used to control the entrance conditions (e.g., minimize cross directional wind intrusion and wind surface separation). The contraction zone was instrumented to accelerate and stabilize air flow with dimensions of 0.3 m wide and 0.08 m high contracting to 0.1 m wide and 0.08 m in height. After the contraction zone, a stabilizing transition section was placed to further focus the wind paths with dimensions of 1.0 m long, 0.1 m wide, and 0.08 m high with all sides enclosed.

Continuing along the flow direction, the working section was the target area where the soil surface is exposed to the wind with dimensions of 0.935 m long, 0.1 m wide, and 0.09 m high (e.g., working section area is 0.0935 m^2). Measuring ports were placed 0.1, 0.5, and 0.9 m away from the transition section, with the purpose to measure the wind velocity at three locations and three heights at each location, as discussed section 3.3. Likewise, the ports were centered in the middle width of the tunnel, for instance in Figure 3.2 above the slot sampler a port can be seen. Regarding the materials used in the wind tunnel frame, rigid PCV foam sheets were chosen because they could be cut and manipulated with a standard utility knife and were relatively

lightweight.

(a) (b)

Figure 3.1. Pictures of the: (a) downwind view of the Portable Wind Tunnel (PWT) system; and (b) top view of its contraction section.

Figure 3.2. Frontal view of the slot sampler.

Originally, a gate valve was constructed to transition the working section of rectangular shape to circular shape to connect to the primary suction fan; however, it also provided the regulation of wind speeds with the use of a vertical sliding plastic plate that made the gate valve.

The control valve or gate valve was connected to the primary suction fan with ventilation ducting; also, the primary fan had to be custom fabricated with sheet steel to adapt to the diameters from the ducting to the fan. The primary suction fan was a 370-W 220-V motor and had a diameter of approximately 0.3 m and an air flow capacity of 2300 m^3 hr^{-1}.

Samples of erosion were collected by the slot sampler (Figure 3.2) that was oriented vertically as a slot to collect a portion of the erosion; moreover, the slot sampler was used to ensure that the primary suction fan was not restricted. From the beginning to the end of a test, the slot sampler collects samples into a container to then be weighed to determine the amount of erosion. The slot sampler was positioned at the end of the working section stretching from the ground to the top of the tunnel and occupies 0.065-m-long ground cover (e.g., the total length of the slot sampler and working section equals to 1.0 m). The slot sampler was 0.01 m wide and 0.08 cm high, resulting in a frontal area of 8.86% of to the total cross-sectional flow area (0.1 m by 0.09 m) with the bottom enclosed with a PVC foam sheet. Assuming the working section as uniform erosion and only sampling erosion the equivalent amount of total erosion is 11.25 times the erosion amount collected. The top of the slot sampler is open and connected via schedule 40 PVC tube to the collection container; here particles are filtered by the collection container shown on the right-hand side of Figure 3.3. Connections of PVC tube were connected with couplings and 45° elbows to minimize restrictions.

Within the collection container, a filter arrangement was as follows in the flow direction: chamber for settling, metal divider, filter paper, metal screen, and PVC foam sheet spacer. The main body of the collection container was a stainless-steel closable container measuring approximately 0.1 m in diameter (Figure 3.3a). This figure also shows the chamber for settling that is the bottom larger portion of the collection container, which provides a space for lower

velocity encouraging settling. The use of the metal screen is to support the filter paper from ripping as shown in Figure 3.3b. To keep the filter paper in position, a PCV foam spacer was added to the top side of the metal screen to give a tight fit and help seal the filter paper to the metal divider. On either side of the collection container, a union connection is installed to enable quick and effective removal of the container and the erosion sample. Then, exiting the collection container is the collection suction fan, which has a capacity of 168 m^3 hr^{-1} air flow. The air flow of collection fan is controlled by a ball valve between the slot sampler and the collection container. The PWT is powered by a seven-horsepower single-phase gasoline generator with outputs of 4000 watts and 220 volts.

(a) (b)

Figure 3.3. Pictures of the: (a) collection container; (b) filter scheme.

Additional items used during tests were a digital hot-wire anemometer, moisture meter, duct tape, and sample containers. The wire anemometer was used to measure the wind velocity at three given heights within the working section. Likewise, the hot-wire anemometer displayed real-time velocity in meters per second and was observed and recorded accordingly. Before

testing and for refence, the soil was probed to get relative moisture for comparison only as the instrument was not calibrated to be accurate (Table 3.1). To simplify transport and create seals between connection points on the PWT, duct tape was used for a quick and practical application.

Table 3.1. The field test data.

Test #	Wind Speed u (m/s)	Collected Erosion (g)	Water Content ω (%)	Soil Moisture **θ** (%)	Silt and Clay Content (%)
1.1	4.80	0.02	1.2	7.1	9.709
1.2	4.80	0.02	1.2	7.1	9.709
2.1	3.77	0.15	0.7	4.6	12.456
3.1	3.70	0.32	0.2	3.1	7.602
4.1	5.63	1.58	0.4	3.6	14.286
5.1	5.17	0.67	0.3	3.3	8.357
6.1	5.10	1.53	0.3	3.3	9.708
7.1	4.47	0.65	0.4	3.6	12.680
8.1	3.43	6.34	0.5	2.0	21.753
9.1	4.47	3.53	0.4	2.7	17.500
10.1	3.87	2.83	0.4	3.0	14.696
11.1	3.83	0.23	0.8	2.6	18.893
12.1	4.63	1.17	0.6	3.5	16.038
13.1	4.13	0.54	0.4	4.0	14.760
14.1	4.03	0.61	0.5	3.5	16.149
15.1	4.73	0.49	0.7	3.6	10.462
16.1	4.77	1.68	1.0	4.0	20.930
17.1	4.80	1.29	0.9	3.5	27.243
18.1	6.63	1.8	0.7	3.5	22.006
19.1	3.97	1.9	0.6	4.2	15.244
20.1	5.17	4.02	0.5	6.0	13.354
21.1	5.00	1.31	0.5	6.0	13.514
22.1	4.33	4.08	0.6	6.0	12.424
23.1	5.30	0.35	2.0	5.0	16.077
24.1	5.93	0.23	3.1	5.2	18.794
25.1	5.53	0.46	1.1	4.2	11.437
26.1	4.93	0.63	1.2	7.1	8.480
27.1	5.30	0.26	1.4	8.3	8.500
28.1	5.23	0.91	1.2	9.4	8.500
29.1	5.60	1.2	0.9	6.8	8.500
30.1	5.13	0.94	0.8	6.6	8.500

3.3 Data Collection

For each of the 31 respective test locations presented in Table 2.1, the PWT was tested for a varying duration, while observing the wind velocity, then collecting eroded particles and ground surface samples. Tests were found to generally be consistent and relative with both the ball valve and gate valve fully open. The test durations for the first 3 tests (labeled 1.2, 1.2, and 2.1 in Table 3.1) were 6.33, 10, and 15 minutes, respectively, with the remaining tests having a duration of 20 minutes. At the three measuring ports over the working section, the wind velocity was recorded at 0.006 m from the soil surface (bottom), at the middle height of 0.045 m (effective), and close to the ceiling of the tunnel at 0.084 m (top). The naming of the three ports is successive in the flow direction as the front, middle, and back ports. Furthermore, the other two ports were covered with duct tape when not in use. The wind speeds at the bottom and middle heights were averaged for all three ports and the average wind speed was considered to be the erosive force causing the collected erosion (Table 3.1)

To minimize the disturbance to the soil surface before testing, soil samples were taken after each test. Soil samples were used to determine the soil water content by the oven dried method (ODM) (ASTM D2216-19) and the soil texture by estimating soil texture (e.g., jar settling method) (Whiting *et al.,* 2015). The method of collecting soil samples was by extracting soil from the front, middle, and back port at a depth of 0.5 cm from the entire width of the working section to represent the entire erosion surface. These three-soil samples were then added together as one sample and such soil sample had average initial mass of 130 grams. The ODM was conducted by weighting the soil sample before and after being placed into an oven for 24 hours at 110 °C (Table 3.1) using an electric scale with accuracy to the hundredth, thus the soil mass before and after can be subtracted to get water mass. Note the containers were pre-weighed

and subtracted before calculating water content. The water content was determined by comparing the mass of the water to the mass of the dry soil. The estimate soil texture was performed in a graduated glass cylinder where the same soil sample was used in the water content determination were added with distilled water and shaken until complete mixture, then left to settle for 24 hours (Whiting *et al.,* 2015). The soil was placed into the graduated cylinder and height was recorded. Then, distilled water was added with the soil sample to full and capped. The water and soil were shaken to separate the particles, next after 24 hours of settling markings of soil size heights were recorded. The target soil particle size was that of fines (e.g., silt and clay) and with the height of the fines compared to the total height of soil give the relative percent of eroded materials. As different soil size particles settle at different rates the particles disassociate by size, and form singular heights of soil size. In particular, the relative clay and silt percentage (i.e., target particle size or erodible material) was of interest for the subsequent analysis and modeling (Table 3.1).

3.4 Data from Previous Study

The Chinese collaborators (Luo *et al.*, 2014) did extensive field samplings and subsequent laboratory analyses for soil textures, organic contents, and soil-water parameters. They "…took undisturbed soil columns using stainless-steel cylinder augers (ϕ50.46 mm × 50 mm) from 69 sites randomly positioned across the watershed from 0 to 30 cm and 30 to 60 cm horizons and analyzed the soil samples in the hydrology laboratory of Inner Mongolia Agricultural University (IMAU). For each soil sample, its texture (i.e., percent of sand, silt, and clay) (Bowles, 1992) was determined using standard mechanical sieves (NHRI, 1999) and a Rise-2008 Laser Granulometry (Storti and Balsamo, 2010). The saturated hydraulic conductivity was determined using the method described in Carter and Gregorich (2007), while contents of organic matter and saline ions (e.g., Na^{+}, Ca^{2+}, and Mg^{2+}) were measured by following the

standard Walkley-Black dichromate titration procedures (Schumacher, 2002)."

This study used these data as the references to estimate the actual particle sizes and densities.

3.5 Results and Discussion

The overview of results from the tests were positive where quality wind speeds, soil samples, and records of the data were sufficient. Collected erosion amount ranged from the lowest amount at 2 g and the highest amount at 6.35 g. The average wind speed was 4.78 m s^{-1}, with a range of wind speeds from 3.4 to 6.6 m s^{-1}. Moreover, as expected, the soil water content was relativly dry, with an average of 0.81 % and a range of 0.18 to 3.14 %.

Upon comparison of the wind speed and erosion amount, it was evident that there were two test simulations excluded from the further analyses because of the poor measurement quality and missing values. As shown by the box and whisker plot (Figure 3.4a), for one of these two abandoned tests, there was an extreme outlier in the upper range of more than 18,000 mm $year^{-1}$, which corresponds to being outside the range of 3 times the inner quartile range. Furthermore, the box and whisker plot were plotted from the measured data of total grams converged to erosion rate using bulk density, PWT area, and duration. The locations and means of items in the box and whisker plot are the following: the x is the mean, the bar in the middle of the dark box is the median, the outer bars of the dark box are the inner quartile rages (25 and 75%), the next two bars are corresponding to 9 and 91% ranges, and the filled circles are outlying value. The second of these two abandoned tests did not measure water content (not shown). In the Figure 3.4b, the histogram of simulated wind erosion can be compared to that of the historical histogram (Figure 2.3) concluding that the simulated value is within the range of historical.

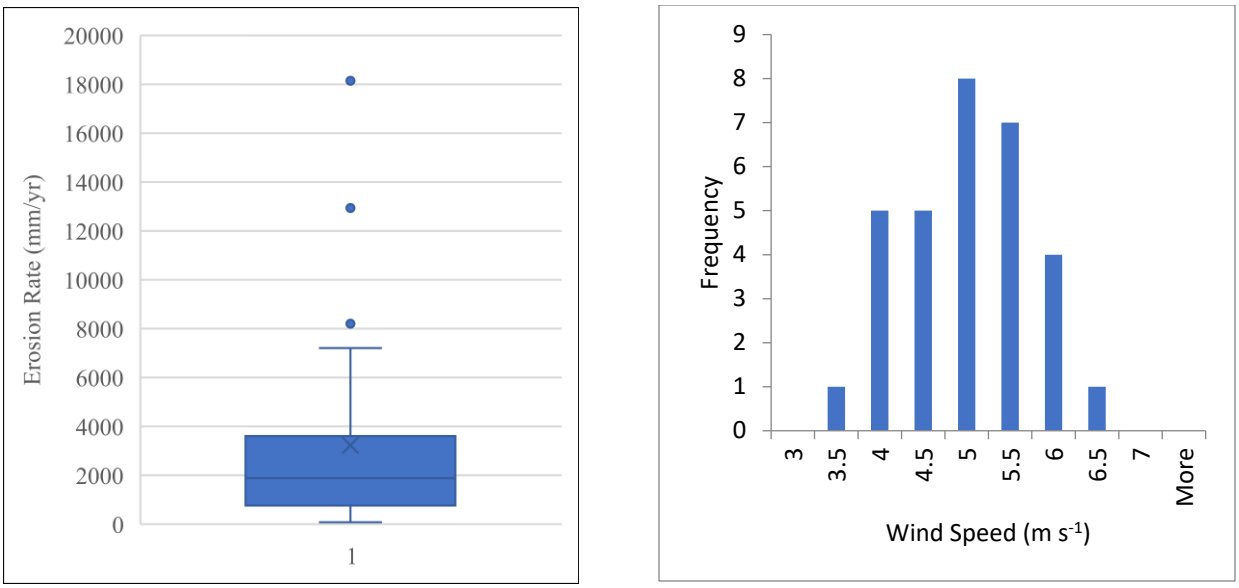

Figure 3.4. a) Box and Whisker plot of the measured erosion rates, and b) histogram of the simulated wind speeds.

The relationship between wind speed and erosion was not strong (Figure 3.5). However, when the water content was compared to the erosion it tended to decrease with increase of soil moisture (Figure 3.6).

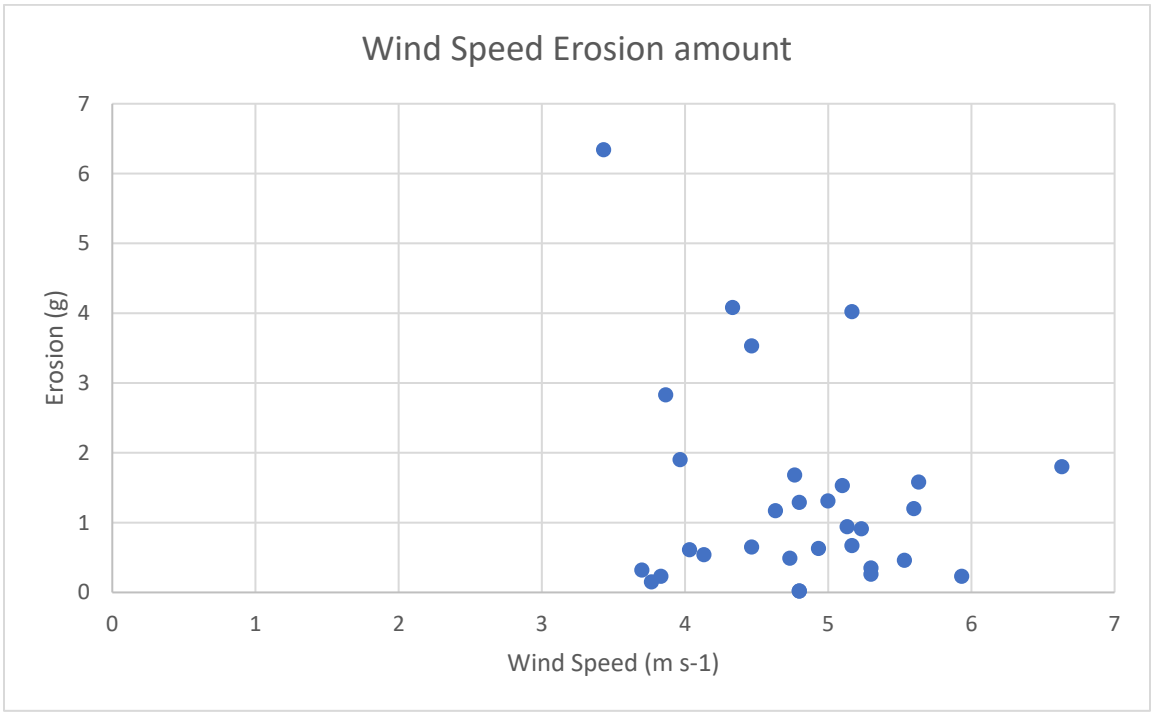

Figure 3.5. Erosion vs wind speed.

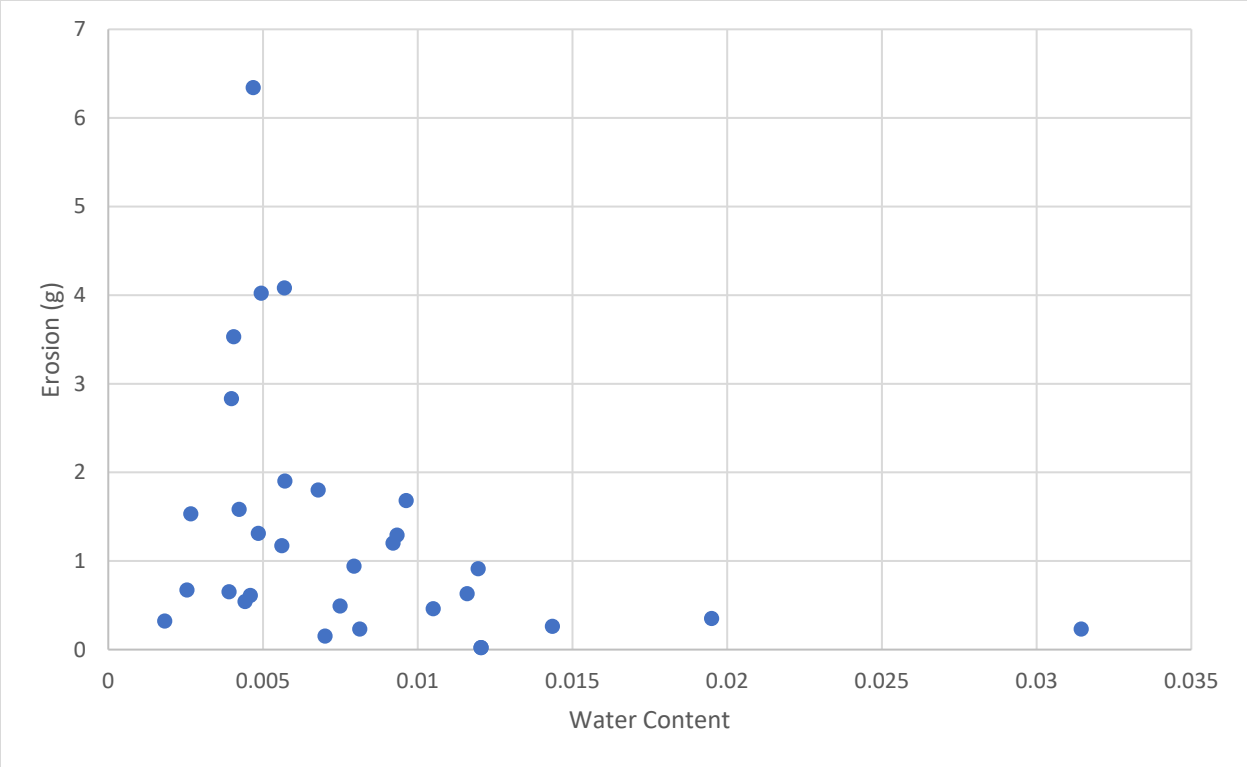

Figure 3.6. Erosion vs water content.

From the wind speeds at the ground, middle, and ceiling heights and in the front, middle, and back port positions, velocity profiles can be made (Figures 3.7, 3.8, and 3.9). The wind speeds at all three ports varied vertically in height and in general the wind speeds were greater at the middle or effective height.

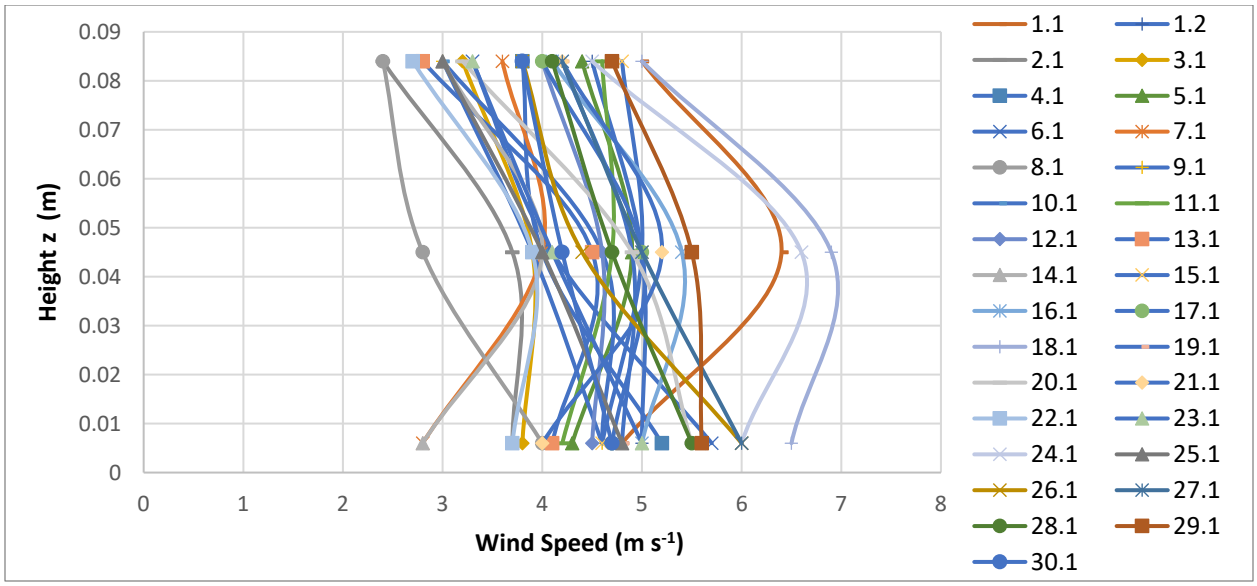

Figure 3.7. Velocity profile at the front port.

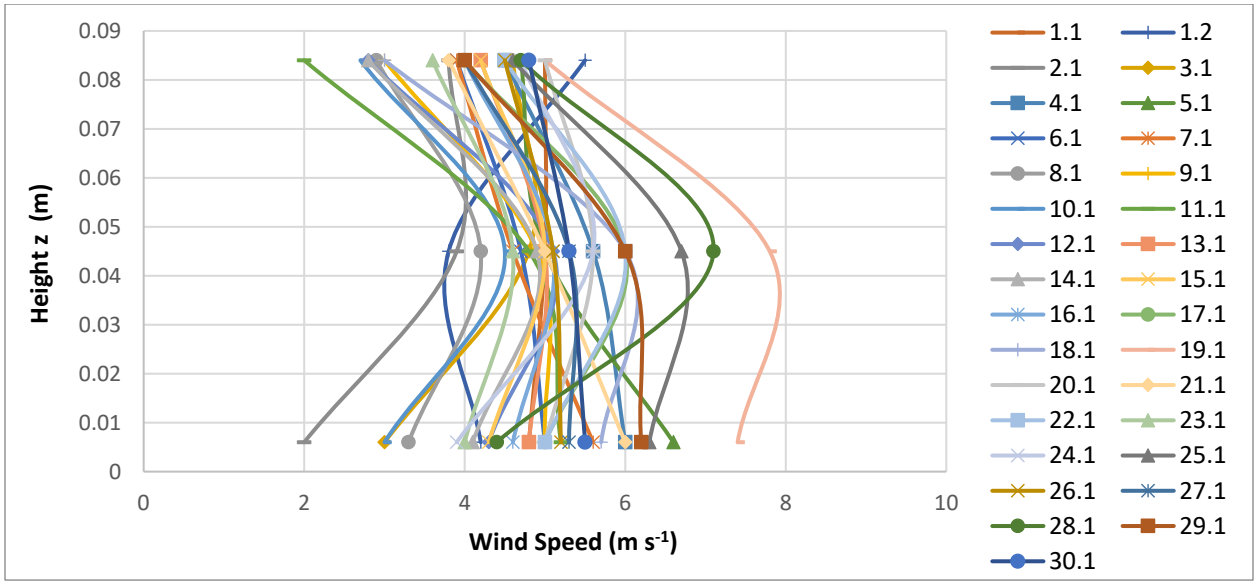

Figure 3.8. Velocity profile at the middle port.

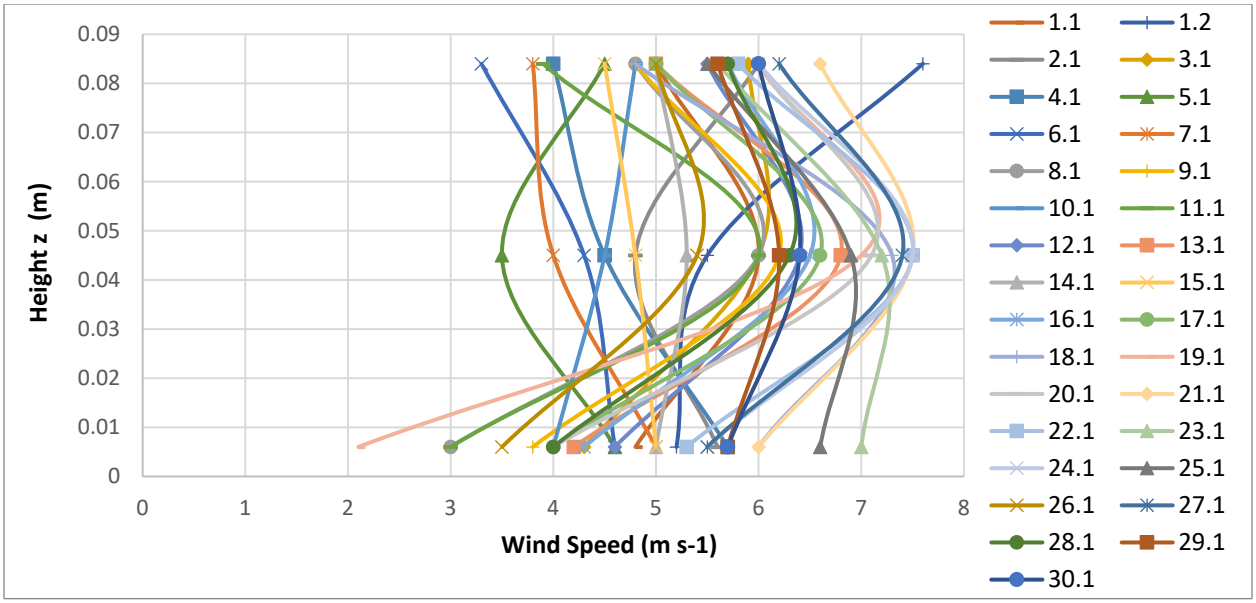

Figure 3.9. Velocity profile at the back port.

Variations in the roughness and or height from the soil surface could have affected the wind speed and wind profile. For the measurement of the wind speed, a more accurate pitot tube is recommended as the hot-wire anemometer relies on the cooling effect to measure the wind speed, thus a significant error could have been problematic. The hot-wire anemometer was a sensitive instrument that had to be operated at an exact height, orientation, and plume to have accurate measurements. Therefore, the hot-wire anemometer had many drawbacks to produce consistency and could have given uncertain wind speeds. Along with the pitot tube, using a data logger would eliminate possible reading errors.

During different stages of construction of the PWT, testing was conducted to ensure quality control over the functionality of the PWT. Initial trial testing of the PWT was held indoors on the carpet to think through the procedure of how to run the testing. Once out in the field, more trials (not shown) were conducted to eliminate problems of further error. Issues that arose were that the circuits of the generator and the axial fan were not compatible due to the wiring of 220-volt. Thus, a new van had to be purchased at a local store and used. Also, the

connection of the working section to the ground was not seamless, so a sheet metal had to be inserted on the outsides of the working section to prevent lateral air inflow and efflux. During testing, since the soil was bare and loose, this enabled the soil to erode out from under the working section walls; the interface at the soil surface between the inside and outside wall of the working section could have been broken by improper sealing of the interface with a metal steel. Thus, the actual wind tunnel needs to be sheet metal and obtain the connection directly as any space dramatically reduces the wind speed. Additionally, the ducting connecting the control valve and the primary fan was not operated in its fully extended position because the ribs created large drag consequently, reducing the wind speed. No trial test data was used for analytical modeling.

Collection of soil samples before testing should have been conducted as there could have been drying effect to the soil from the wind tunnel. The insufficient quanitification of the varying disturbances to the soil structure could have more or less influences on the amount of erosion that was sampled. The disturbances include, but are not limited to, rain wetting-drying cycles and livestock tramplings. In addition, the slot sampler was devised for suspended, but not-saltation, particles. Because of the nature of saltation particles close to the ground surface, however, saltation particles could not be captured by the slot sampler.

Throughout the design, construction, and testing of the PWT system, there were numerous challenges that either influenced or dictated the project. For instance, in starting the construction, it was found that the local readily available selection of building materials was not accessible, which led to the use of the PVC foam sheets rather than sheet metals. The PVC foam sheets were shaped easily, but excessive maintenance was a drawback. With frequent maintenance, the PWT was referred to the term “duct tape wind tunnel” to continue operation.

Conclusively, the PWT system stood the tests of time because of its easiness of assembly, transportation, and many deployments in to the field with repeatability. The small size of the PWT system made it feasible to test both large-size bare soils and patches between large grass clumps.

CHAPTER 4:
MODELING

4.1. Description of IAFP

Combining the resultant field test data with the integrated aeolian and fluvial prediction (IAFP) model was the pinnacle of the research at hand. The IAFP model, developed by Wang *et al.,* (2014a), was to provide a framework of modeling wind and water erosion simultaneously. In a given year, these two types of erosions occur simultaneously though one type may be dominant over another at a specific time, so both need to be evaluated in a single modeling domain to mimic actual situations. However, as part of a three-year research project funded by the National Science Foundation (NSF) International Research Experience for Students (IRES), this study focused on wind erosion from bare soils only.

The IAFP considers many parameters that describe the environment in which the erosion takes place. Such parameters characterize land cover, topology, and soil-water properties (e.g., soil moisture) that are all evaluated in the IAFP governing equation. The erosion modulus (q_a) is the acting governing equation that compares the shear stress of the effective wind speed and the threshold dynamic of soils and land cover, which are independent of land cover for bare soils. q_a is computed as:

$$q_a = C_a \left(\frac{\tau_* - \tau_{*c}}{\rho_{air}}\right)^{\frac{3}{2}} \quad (1)$$

where q_a is the wind erosion modulus (g m^{-2} s^{-1}); C_a is the soil-specific coefficient of wind erosion when the surface soil is bare and dry (g m^{-5} s^2); τ_* is the effective wind shear stress (N m^{-2}); τ_{*c} is the threshold wind shear stress (N m^{-2}); and ρ_{air} is the density of air (kg m^{-3})(Chepil 1956, and Marshall 1971).

To apply Eq. (1) to a site of interest, C_a and τ_{*c} need to be determined using measured

data. For bare soil surfaces, τ_{*c} depends on soil properties (namely texture, structure, and particle size) and soil water content, while for vegetated surfaces, τ_{*c} also depends on physiological characteristics of the vegetation (e.g., population density and stem height). τ_{*c} is computed as:

$$\tau_{*c} = \rho_{air} \cdot (u_{*\theta\lambda})^2 \quad (2)$$

where $u_{*\theta\lambda}$ is the threshold surface friction shear velocity (Bagnold, 1914).

For bare soil surfaces, $u_{*\theta\lambda}$ is same as $u_{*\theta}$, which is computed as:

$$u*\theta = fw \cdot u*\psi u_{*\theta} = f_w \cdot u_{*\psi} \quad (3)$$

where f_w is the dimensionless coefficient reflecting the surface soil moisture; and $u_{*\psi}$ is the threshold friction shear velocity when the soil surface is bare and dry (Fécan et al., 1999).

f_w is computed as:

$$f_w = \begin{cases} 1 & if\ \omega \le \omega' \\ \sqrt{1 + 1.21 \cdot (\omega - \omega')^{0.68}} & if\ \omega > \omega' \end{cases} \quad (4)$$

where ω is the mass water content of the surface soils; and ω′ is the threshold water content that depends on the clay content of the surface soils (Fécan et al., 1999).

ω′ is computed as:

$$\omega' = 0.0014 \cdot \left(P_{clay}\right)^2 + 0.17 \cdot P_{clay} \quad (5)$$

where P_{clay} is the clay content, in percent, of the surface soils ((Fécan et al., 1999).

Given ω and bulk density, the soil moisture (i.e., volumetric water content) can be calculated as:

$$\theta = \frac{\rho_b \cdot \omega}{\rho_w (1+\omega)} \quad (6)$$

$$\rho_b = \frac{\rho_s}{1+e} + \rho_w \cdot \theta \quad (7)$$

$$\rho_b = \frac{\rho_s (1+\omega)}{1+e} \quad (8)$$

where θ is the moisture of the surface soils; ρ_w is the density of water (kg m^{-3}); ρ_s is the soil particle density (kg m^{-3}); ρ_b is the bulk density (kg m^{-3}); and e is the void ratio of the surface soils ((Todd and Mays, 2005 and Charbeneau, 2006)). For sandy soils like those in the Balagaer River watershed, the typical value of e = 0.71 was used in this study (Wang *et al.,* 2014b).

$u_{*\psi}$ is computed as:

$$u_{*\psi} = \sqrt{\frac{a_1}{\rho_{air}} \cdot \left(\rho_s \cdot g \cdot d_s + \frac{a_2}{d_s}\right)} \tag{9}$$

where a_1 = 0.0123 (dimensionless) and a_2 = 0.0003 kg s^{-2} are constant coefficients; d_s is the mean diameter of surface soil particles (m); and g = 9.81 m s^{-2} is the gravitational acceleration (Shao and Lu, 2000).

On the other hand, τ_* depends on wind speed and soil surface roughness for bare soil surfaces while also on the physiological characteristics of the vegetation for vegetated surfaces. τ_* is computed as:

$$\tau_* = \rho_{air} \cdot (u_*)^2 \tag{10}$$

where u_* is the surface friction shear velocity (m s^{-1}) (Marshall, 1971).

For bare soil surfaces, u_* is estimated as:

$$u_* = \frac{\kappa \cdot u}{\ln\left(\frac{z}{z_0}\right)} \tag{11}$$

where κ = 0.41 is the von Karman constant; u is the effective wind speed at z distance above the soil surface; and z_0 is the surface roughness height Lyles and Allison, 1975 and Wolfe and Nickling, 1993).

z_0 can be estimated as (Chen *et al.,* 1996 and Dong *et al.,* 2002):

$$z_0 = \begin{cases} 0.5 \cdot d_s & if\ \omega \leq 4.5\% \\ 6144.1 \cdot \omega^{-6.1} \cdot d_s & if\ \omega > 4.5\% \end{cases} \tag{12}$$

4.2. Parameterization of the IAFP Model

This study assumed that ρ_s = 2650 kg m^{-3}, ρ_w = 1000 kg m^{-3}, ρ_{air} = 1.21 kg m^{-3}, e = 0.7153, and d_s = 0.00015 m.

C_a was estimated using the *in-situ* measurements and then scaled up to the watershed. Firstly, by specifying an arbitrary value of C_a, for each of the field tests, Equation (1) was used to estimate q_a. The squared error (SE) was computed as the difference between the estimated and measured values. Also, for all field tests, the sum squared error (SSE) was computed as the summation of the squared errors. Further, the SSE was minimized by adjusting C_a. The calculations were implemented in an Excel® spreadsheet with the adjustment done using Solver®. This resulted in C_a = 5.51 g m^5 s^{-1}. Secondly, the *in-situ* C_a value was scaled up to the Balagaer River watershed as $(5.51\ \text{g m}^5\ \text{s}^{-1}) \cdot \sqrt{\frac{0.0935\ m^2}{5350\ km^2 \cdot 10^6 \frac{m^2}{km^2}}} = 0.23 \times 10^{-4}$ g m^5 s^{-1}, where 0.0935 m^2 is the open bottom area of the PWT working section (section 3.1), and 5350 km^2 is the drainage area of the Balagaer River watershed.

For an area of interest, the estimated q_a can be converted into the corresponding erosion rate using the formula expressed as:

$$ER = 3.1536 \times 10^{13} \frac{q_a \cdot A}{\rho_b} \quad (13)$$

where ER is the soil erosion rate (mm yr^{-1}); A is the area (km^2); and ρ_b is the bulk density of the surface soils (kg m^{-3}).

In terms of C_a = 5.51 g m^5 s^{-1}, the *in-situ* measured soil erosion rates were reproduced using Equation (1). The plot showing the estimated versus measured soil erosion rates (Figure 4.1) indicates a close one to one performance of the model, which can be further verified by a unit linear regression slope and a large coefficient of determination R^2 = 0.74.

4.3. Hypothetical Scenarios and Predicted Erosion Rates

Upon parameterized, the IAFP model was used to predict potential erosions of various hypothetical scenarios for the Balagaer River watershed. In winter and spring (December to March), the watershed has almost zero vegetation coverage, while the soil water content is very low, but the wind speed is relatively high. Herein, the scenarios and predicted erosion rates can reflect the situations in these two seasons. Four scenarios, designated Scenario I through IV for description purposes, were analyzed in this study. Scenario I assumed a constant wind speed of 4.8 m s^{-1} while water contents varying from 0 to 6% and a constant ρ_s = 2650 kg m^{-3}; Scenario II assumed wind speeds varying from 0 to 15 m s^{-1} while a constant water content of 0.2, 2, 3, 4, or 5% and a constant soil particle density ρ_s = 2650 kg m^{-3}; Scenario III assumed a constant wind speed of 4.8 m s^{-1} and a constant water content of 4%, while soil particle densities varying from 2600 to 2750 kg m^{-3}; and Scenario IV assumed historical wind speeds and soil moistures at a 10-cm depth while a constant ρ_s = 2650 kg m^{-3}.

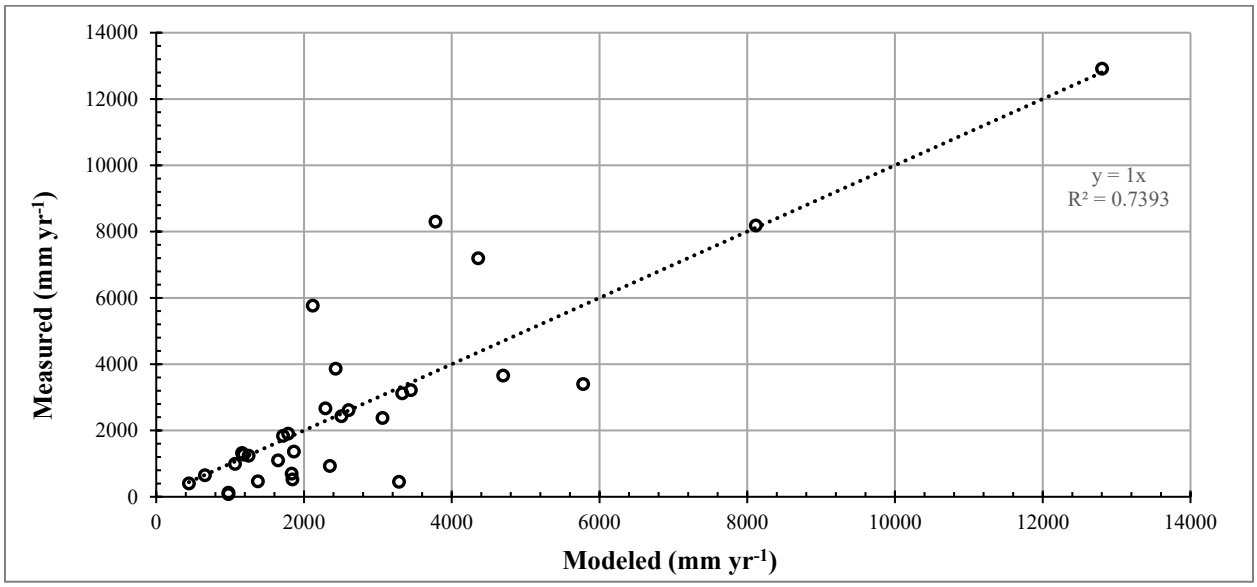

Figure 4.1. The modeled versus measured soil erosion rates by the portable wind tunnel (PWT).

For Scenario I: Changes in climate have been cited to have direct and or indirect

impacts on the environment such as meteorological factors, and subsequent effects on soil water content, wind speed, vegetation cover, and land use. The evaluation of scenario analysis of critical parameters can provide a clear insight into the limits and trends of how erosion occurs under different constraints. Unlike the case of calibrating the model, as modeled in section 4.2, the scenario analysis was conducted by assuming a constant wind speed of 4.8 m s^{-1}, percent clay of 8%, a water content of 4%, and wind speed height of 0.045 m. However, the water content was arbitrarily varied from 0 to 6%.

As expected, the predicted soil erosion rate tended to decrease with an increase in water content (Figure 4.2). The erosion rate was predicted not to be very sensitive to the variation of water content if it is less than 1.5%. This can be because the potential erosion rate, which is controlled by wind speed and independent of the soil conditions, has been reached for such a low water content. If the water content ranges from 1.5 to 4.5%, the predicted erosion rate tended to decrease at 0.00028 mm yr^{-1} per unit percent increase of water content, whereas if the water content is higher than 4.5%, the predicted erosion rate would be exponentially decreasing with an increase of water content and become zero at a water content of 5.6%.

The surface soils of the field tests had water contents of 0.2 to 3.1%, with a mean of 0.8% and a standard deviation of 0.73%. This might be the reason for the measured erosion rates had a small to mediate variation (Figure 4.1 and Table 3.1).

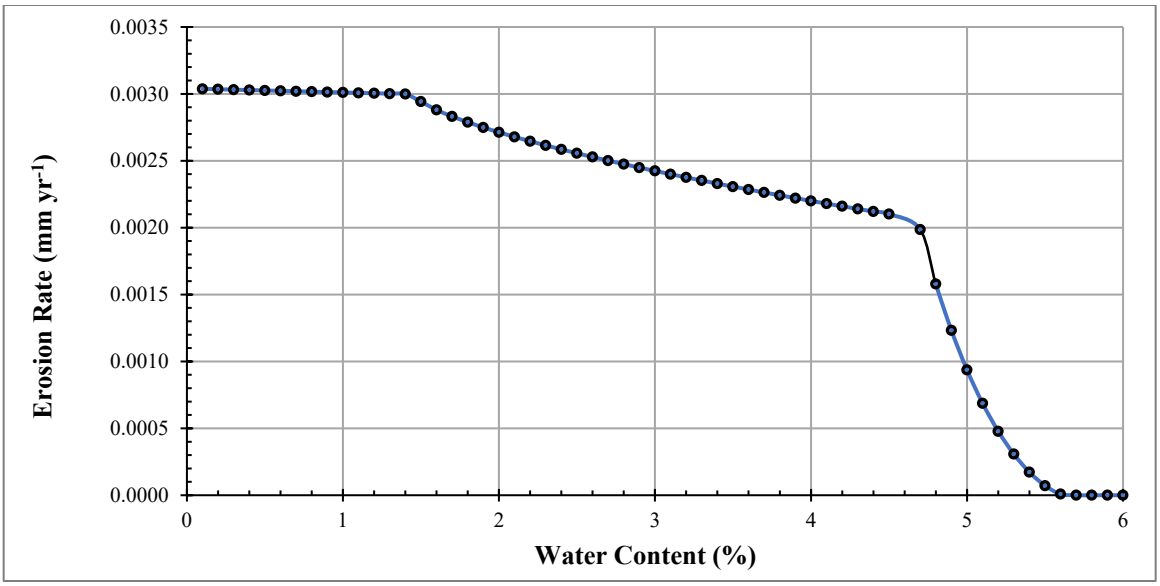

Figure 4.2. The predicted erosion rate versus hypothetical soil water content (u = 4.8 m s^{-1}).

For Scenario II: To assess the influences of wind speed on predicted erosion rate, for each of the selected five soil water contents of 0.2, 2, 4, 5, and 6%, the wind speed was arbitrarily varied from 0 to 15 m s^{-1}. As shown in Figure 4.3, for wind speeds of less than 4.8 m s^{-1}, the erosion rates were predicted to be similar regardless of soil water contents, whereas for wind speed of larger than 4.8 m s^{-1}, the erosion rate was predicted to have a steeper increase for a lower than a higher soil water content (Figure 4.3). For a given water content, the erosion rate was predicted to increase exponentially with an increase in wind speed. If the water content is less than 4%, the predicted erosion rate would increase by 0.065 mm yr^{-1} per 1 m s^{-1} increase of wind speed, while if the water content is higher than 5%, the predicted erosion rate would increase by 0.03 mm yr^{-1} per 1 m s^{-1} increase of wind speed.

The field tests used wind speeds between 3.4 to 6.6 m s^{-1}, with a mean of 4.78 m s^{-1} and a standard deviation of 0.73 m s^{-1}. This might be the reason for the measured erosion rates had a mediate variation with wind speed regardless of the soil water contents (Table 3.1).

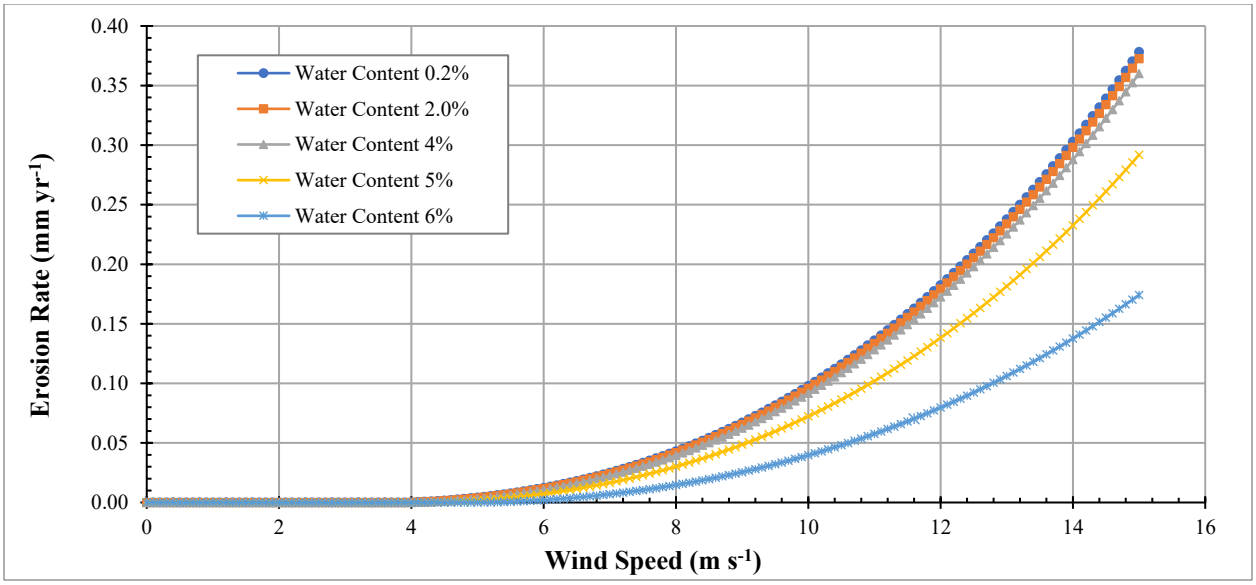

Figure 4.3. The predicted erosion rate versus hypothetical wind speed for various water contents.

For Scenario III: To assess the possible effects of soil parent materials on soil erosion, the soil particle density was arbitrarily varied from 2600 to 2750 kg m^{-3}. As expected, the erosion rate was predicted to decrease with an increase in soil particle density (Figure 4.4). The erosion rate would increase by 3×10^{-6} mm yr^{-1} per 1 kg m^{-3} decrease of soil particle density. At the average density of 2650 kg m^{-3}, the erosion rate was predicted to be 0.003 mm yr^{-1}.

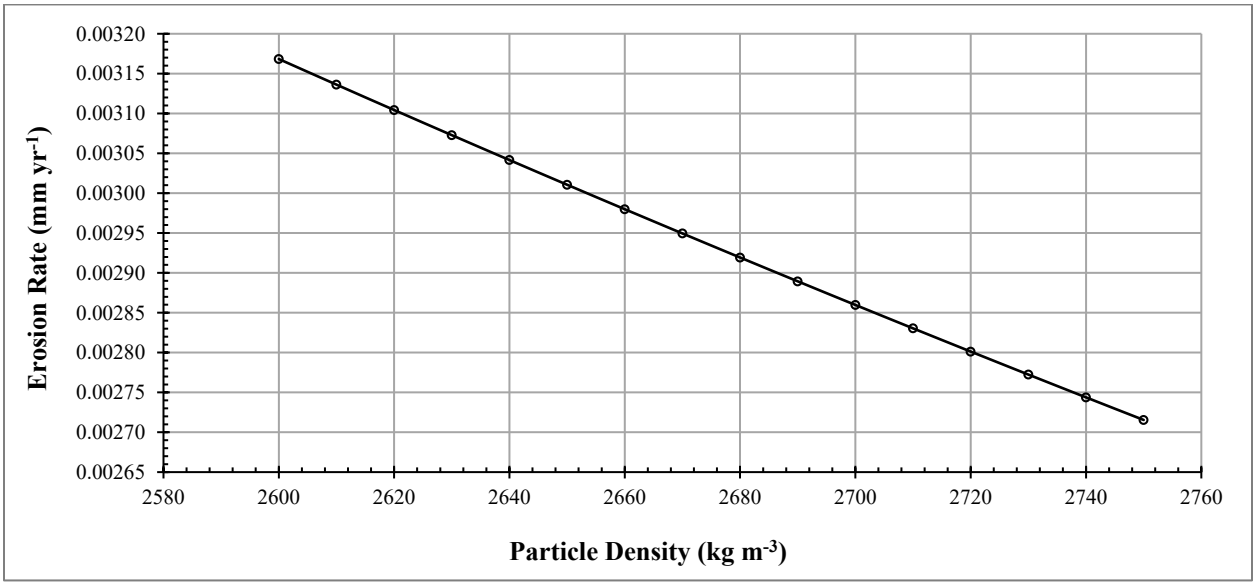

Figure 4.4. The predicted erosion rate versus hypothetical particle density (u = 4.8 m s^{-1}).

For Scenario IV: The long-term data on wind speed and soil moisture at a sensor-based station in the study watershed indicate that high wind speed and a low soil water content moisture tended to co-occur in March and April (Julian days from 90 to 150) (Figure 4.5). The soil moistures (Figure 4.5a) were converted into the responding water contents (Figure 4.5b) using Equation (6) by assuming a soil bulk density of ρ_b = 2650 kg m^{-3} and a water density of ρ_w = 1000 kg m^{-3}. Because the moisture sensor was positioned at a depth of 10 cm below the ground surface, the soil moistures and water contents of the surface soils were much smaller than the values shown in Figures 4.5a and 4.5b, respectively.

As mentioned in Chapter 2 and shown in Figure 4.5, the higher wind speed and lower soil moisture in the early months of a year (winter and spring) were favorable to inducing topsoil erosion. By assuming that soil moistures of the surface soils were the same as those at the 10-cm depth, the erosion rates were predicted using the model. The results are shown in Figure 4.6.

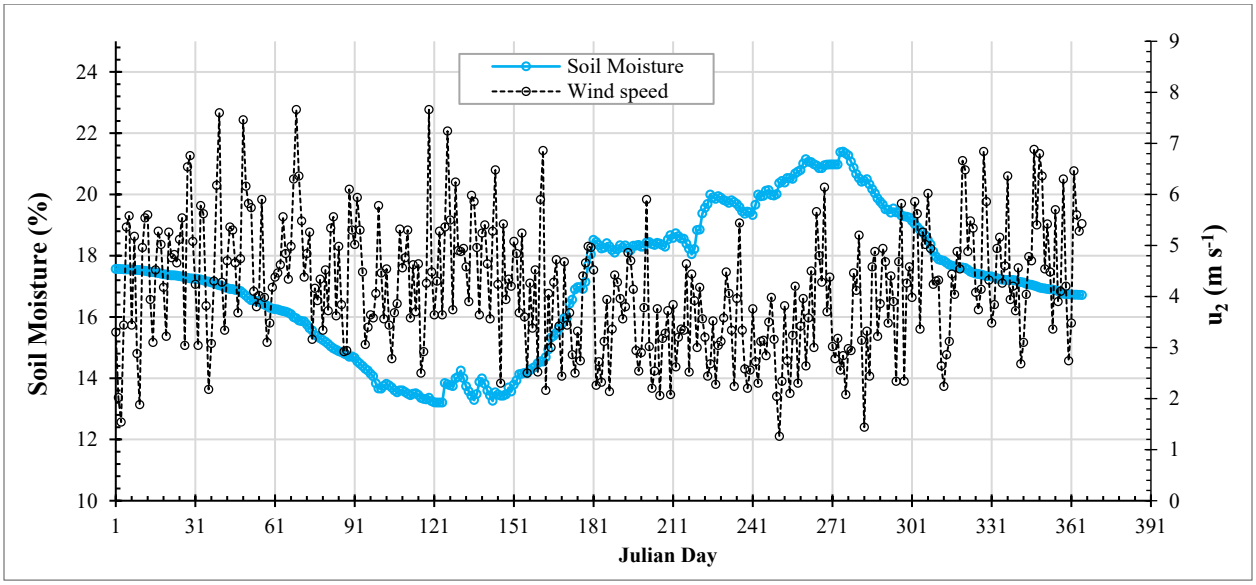

(a)

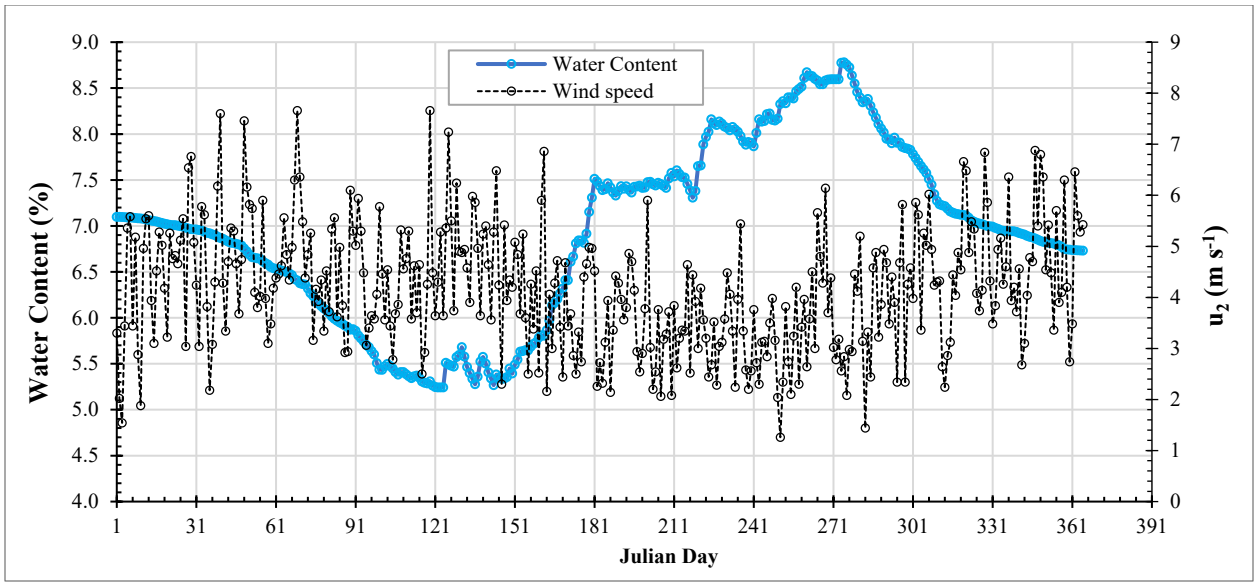

(b)

Figure 4.5. Plot showing the: (a) annual average daily soil moisture and wind speed; and (b) annual average daily water content and wind speed. The record period is from 1 January 2006 to 31 December 2010. The wind speed (u_2) was measured at 2 m above the ground surface.

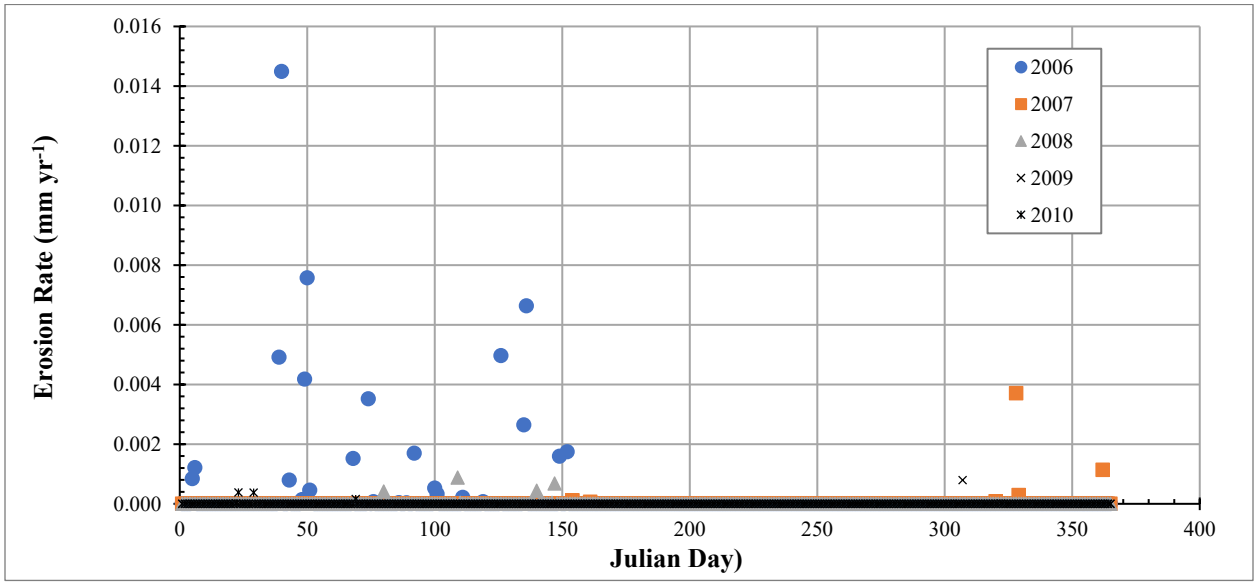

Figure 4.6. The predicted historical daily erosion rates for the Balagaer River watershed.

4.4 Discussion

The tests conducted at 31 sites provided the *in-situ* data on wind speed, water content, and erosion under dry and bare conditions to calibrate the IAFP model for the Balagaer River

watershed. The measured wind speed ranged from 3.4 to 6.6 m s^{-1}. The watershed model calibration resulted in $C_a = 0.23 \times 10^{-4}$ g m^5 s^{-1}, which is about 20 times smaller than the value (4.6×10^{-4} g m^5 s^{-1}) presented by Wang *et al.* (2014b). Because this study used the site-specific data, it was logically considered that 0.23×10^{-4} g m^5 s^{-1} is more applicable for the Balagaer River watershed.

For the study watershed, the threshold water content was determined to be 6%, which is equivalent to the soil moisture of about 15%. If the soil moisture is lower than this threshold, the erosion rate would exponentially increase (Figure 4.2). Wang *et al.* (2014b) reported a threshold soil moisture of 25% if the watershed has the "existing" vegetation coverage. The main reason for such a difference can be attributed to the difference C_a values. In addition, at the threshold soil moisture, the threshold wind speed was determined to be 4.0 m s^{-1} (Figure 4.3). Such a soil-water and weather condition are very common in March and April (Figure 4.5) for the study water, implying that wind erosion in spring can be a serious concern. On average, under the historical conditions, the wind erosion rate was predicted to vary from 0.001 to 0.015 mm yr^{-1}, with a mean of 0.003 mm yr^{-1}. This means that the watershed could lose 16,050 m^3 topsoil per year, which is equivalent to about 16,100 tonnes per year. The topsoil is vital for efforts to sustain grasslands because it is loose and has a plentiful supply (Wang *et al.*, 2014c). Losing the topsoil will likely trigger irreversible degradation of the grasslands of the Balagaer River watershed.

As a result of climate change, the precipitation to be received by the Balagaer River watershed will be significantly decreasing (Wang *et al.*, 2014c), implying that the study watershed would incur more frequent and larger magnitude topsoil loss from wind erosion in the future. This is also likely true for the Eurasian Steppe (or Great Steppe), which shares a similar

climate with the study watershed with climate change obviously happening. The Great Steppe is the vast steppe ecoregion of Eurasia in the temperate grasslands, savannas, and shrublands biome. It stretches from Bulgaria, Romania, and Moldova through Ukraine, Russia, Kazakhstan, Xinjiang, and Mongolia to Manchuria, with one major exclave, the Pannonian steppe or Puszta, located mostly in Hungary and partially in Serbia and Croatia. Thus, the results of this study can serve as the key scientific information for developing practical measures to better protecting and utilizing the fragile steppe resources.

CHAPTER 5:
CONCLUSIONS

A Portable Wind Tunnel System (PWT) was devised in accordance with the needs and focus of the project. Because of the large drainage area of the Balagaer River watershed, it is costly prohibitive, technically impractical, and logistically infeasible to use a laboratory wind tunnel to conduct a number of tests on *in-situ* soil samples in a manageable time period. In this regard, the PWT proved to be superior to the laboratory wind tunnel.

The PWT was effectively deployed at typical sites across the watershed to conduct quick tests with a minimal disturbance because of its small footprint which facilitated the use both in open areas and restricted spaces between large grass clumps. The sites had bare surface soils with varying topographic gradients and water contents. The data from the tests were used to parametrize and calibrate an IAFP model, leading to $C_a = 0.23 \times 10^{-4}$ g m^5 s^{-1} at the watershed scale. The calibrated model predicted that the study watershed might have an annual loss of 16,050 m^3 topsoil, which is equivalent to about 16,100 tonnes, under the historical climate conditions. In the future, as a result of climate change, the watershed would have a larger erosion rate. As a reasonable generalization, the results of this study can serve as the key scientific information for developing practical measures to better protecting and utilizing the fragile steppe resources.

CHAPTER 6:
RECOMMENDATIONS FOR FUTURE RESEARCH

The next two phases of the project should use the portable wind tunnel (PWT) system to collect data at more sites with bare surfaces to verify the findings of this study. In addition, PWT tests should be conducted to collect data at sites with varying vegetation coverage conditions. Such data will be used to parameterize the IFAP model to examine effects of vegetation on topsoil erosion. These additional tests should have water contents, wind speeds, and soil densities that are equal to and/or larger than their upper limits of 6% (Figure 4.2), 15 m s^{-1} (Figure 4.3), and 2750 kg m^{-3} (Figure 4.4) used in the modeled scenarios of this study. This will make it possible to minimize the prediction uncertainties resulting from extrapolation of the test data. Further, the calibrated IFAP model should be used to simulate various scenarios to determine the threshold of vegetation coverage under which wind erosion will likely trigger an irreversible degradation of the steppe grasslands. Moreover, the PWT system needs to be improved to generate more uniformly-distributed laminar air flows. The additional improvements to the PWT system may include building the actual frame out of entirely metal and increasing the open area of the slot sampler to capture more percent of eroded soils.

APPENDIX

STATISTICS OF THE AVERAGE DAILY WIND SPEEDS FROM 1955 TO 2010

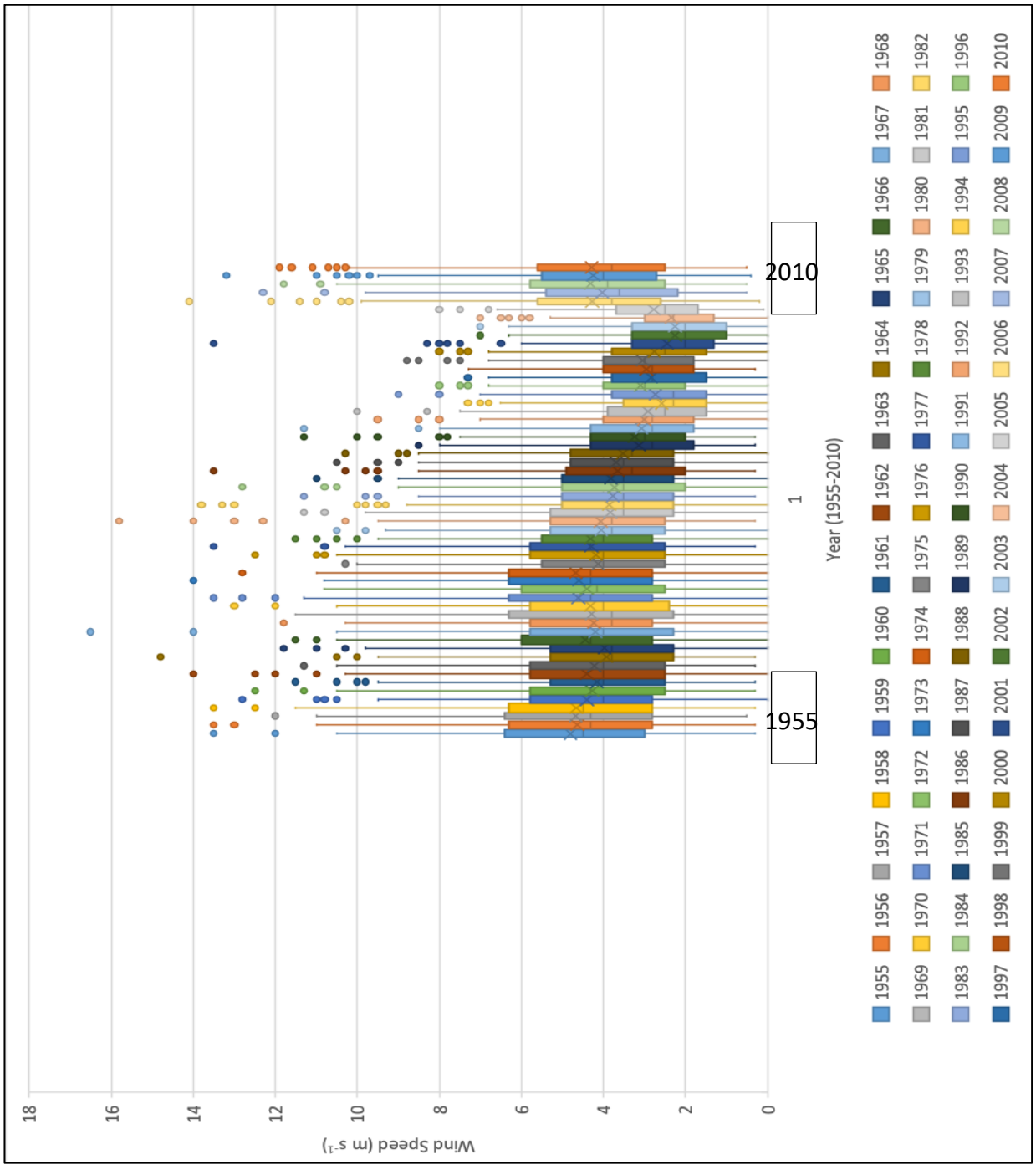

REFERENCES

ASTM D2216-19, (2019). Standard Test Methods for Laboratory Determination of Water (Moisture) Content of Soil and Rock by Mass. ASTM International, West Conshohocken. PA. www.astm.org

Bagnold RA. (1941). The Physics of Blown Sand and Desert Dunes. Methuen: London; 265.

Bowles, J.E., 1992. Engineering Properties of Soils and Their Measurement. New York, NY: McGraw-Hill.

Carter, M.R., Gregorich, E.G., (eds.), 2007. Soil Sampling and Methods of Analysis (2nd ed.). Boca Raton, FL: CRC Press.

Charbeneau RJ. Groundwater Hydraulics and Pollutant Transport. Waveland Press, Inc.: Long Grove, IL

Chen, Zhibao, Zhenshan, & Zuotao. (1996). Wind tunnel test of the influence of moisture on the erodibility of loessial sandy loam soils by wind. Journal of Arid Environments, 34(4), 391-402.

Chepil WS. (1956). Influence of moisture on erodibility of soil by wind. Soil Science Society of America Proceedings 20: 288–292.

Dong Z, Liu X, Wang X. (2002). Wind initiation thresholds of the moistened sands. Geophysical Research Letters 29(12): 1585.

FAO (Food and Agriculture Organization of the United Nations). (2008). Harmonized World Soil Database (version 1.0).

Fécan F, Marticorena B, Bergametti G. (1999). Parameterization of the increase of the Aeolian erosion threshold wind friction velocity due to soil moisture for arid and semi-arid areas. Annales Geophysicae 17: 149–157.

Guo, B., Zhang, F., Yang, G., Sun, C., Han, F., & Jiang, L. (2017). Improved estimation method of soil wind erosion based on remote sensing and geographic information system in the Xinjiang Uygur Autonomous Region, China. Geomatics, Natural Hazards and Risk, 8(2), 1752-1767.

Ishizuka M, Mikami M, Yamada Y, Zeng F, Gao W. (2005). An observational study of soil moisture effects on wind erosion at a Gobi site in the Taklimakan Desert. Journal of Geophysical Research 110: D18S03. Kirkbride MP, Reeves AD. 1993. Soil erosion caused by low- intensity rainfall in Angus, Scotland. Applied Geography 13: 299–311.

Lancaster, N., & Baas, A. (1998). Influence of vegetation cover on sand transport by wind: Field studies at Owens Lake, California. *Earth Surface Processes and Landforms, 23*(1), 69-82.

Li, Kang, Zhang, Zhao, Shirato, & Taniyama. (2005). Changes in intensity of wind erosion at different stages of degradation development in grasslands of Inner Mongolia, China. Journal of Arid Environments, 62(4), 567-585.

Luo Yanyun, Xixi Wang, Fengling Li, Ruizhong Gao, Limin Duan, Tingxi Liu. 2014. Responses of grass production to precipitation in a mid-latitude typical steppe watershed. Transactions of the ASABE. 57(6): 1595-1610.

Lyles L, Allison B. (1975). Wind erosion: uniformly spacing nonerodible elements eliminates effects of wind direction variability. Journal of Soil and Water Conservation 30(5): 225–226.

Marshall JK. (1971). Drag measurements in roughness arrays of varying density and distribution. Agricultural Meteorology 8: 269–292.

Meng, Z., Dang, X., Gao, Y. et al. J. Arid Land (2018) 10: 534. https://doi.org/10.1007/s40333-018-0059-1.

Musick HB, Gillette DA. (1990). Field evaluation of relationships between a vegetation structural parameter and sheltering against wind erosion. Land Degradation & Rehabilitation 2: 87–94.

National Intelligence Council, Joint Global Change Research Institute, & Battelle Memorial Institute. Pacific Northwest Division. (2009). China [electronic Resource] the Impact of Climate Change to 2030, a Commissioned Research Report.

NHRI (Nanjing Hydraulic Research Institute), 1999. Standard Methods for Civil Engineering: SL 237-1999. Nanjing, China: Nanjing Research Institute (http://www.nhri.cn).

Nyamtseren MANDAKH, Jamsran TSOGTBAATAR, Doljin DASH, Sodov KHUDULMUR. (2016). Spatial assessment of soil wind erosion using WEQ approach in Mongolia[J]. Journal of Geographical Sciences, 26 (4): 473- 483.

Press, 1992.

Schumacher, B.A., 2002. Methods for the determination of total organic carbon (toc) in soils and sediments. NCEA-C- 1282, EMASC-001. Las Vegas, NV: United States Environmental Protection Agency Environmental Sciences Division National Exposure Research Laboratory.

Shao Y, Lu H. (2000). A simple expression for wind erosion threshold friction velocity. Journal of Geophysical Research 105(D17): 22437–22443 Shao, C., Chen, J., Li, L., Dong, G., Han, J., Abraha, M., & John, R. (2017). Grazing effects on surface energy fluxes in a desert steppe on the Mongolian Plateau. Ecological Applications, 27(2), 485-502.

Storti, F., Balsamo, F., 2010. Particle size distributions by laser diffraction: Sensitivity of granular matter strength to analytical operating procedures. Solid Earth 1(1): 25-48.

Strong, C., Leys, L., Raupach, J., Bullard, F., Aubault, M., Butler, R., & McTainsh, J. (2016). Development and testing of a micro wind tunnel for on-site wind erosion simulations. *Environmental Fluid Mechanics, 16*(5), 1065-1083.

Todd DK, Mays LW. (2005). Groundwater Hydrology, 3rd edn. John Wiley & Sons, Inc: Danvers, MA.

Wang, Li, Gao, Luo, & Liu. (2014a). Predicted NPP spatiotemporal variations in a semiarid steppe watershed for historical and trending climates. Journal of Arid Environments, 104, 67-79.

Wang, X., Yang, X., Liu, T., Li, F., Gao, R., Duan, L., and Luo, Y. (2014c). Trend and extreme occurrence of precipitation in a mid-latitude Eurasian steppe watershed at various time scales. Hydrological Processes 28: 5547-5560. doi: 10.1002/hyp.10054.

Wang, Xixi, Liu, Tingxi, Li, Fengling, Gao, Ruizhong, Yang, Xiaomin, Duan, Limin, . . . Li, Rui. (2014b). Simulated soil erosion from a semiarid typical steppe watershed using an integrated aeolian and fluvial prediction model. Hydrological Processes, 28(2), 325-340.

Whiting, David (CSU Extension, retired), Card, Adrian (CSU Extension). (2015). Estimating Soil Texture. Colorado State University: Master Gardener Extension. http://cmg.colostate.edu/Gardennotes/214.pdf

Wolfe SA, Nickling WG. (1993). The protective role of sparse vegetation in wind erosion. Progress in Physical Geography 17(1): 50–68.

Wu, J, and O L Loucks. The Xilingol Grassland. Washington D.C.: National Academy

CURRICULUM VITA

Education

Old Dominion University - Norfolk, VA

Bachelor of Science in Civil/Environmental Engineering - GPA: 3.78 May 2018

Master of Science in Civil Engineering - GPA: 3.78 May 2018-Present

Concentration: Water Resources/Hydraulics Engineering

FE Exam Passed.

Computer Skills: AutoCAD, MicroStation, GIS, MS Office, MODFLOW2005, and HEC-RAS.

Experience

(VDOT) Internship Environmental Division June-Aug, Dec 2016

- Project land assessment Phase one & two (VDOT liability measure)
- Introduction to project management, scoping, stream restoration designs
- Mitigation for VDOT Projects (bank mitigation credit and VDOT mitigation credit)

(VDOT) Location and Design (L&D) -Hydraulics Division June-Aug, Dec 2017

- MicroStation tasks (drainage areas, pre/post development areas)
- Culvert and Ditch analysis computations, Nutrient Credits calculations
- FEMA FIRMete maps for site projects

(VDOT) Internship Computer programs

- **Micro Station –** Computer drafting and design program
- **Ditch Spreadsheet-** Computations for Erosion control measures
- **Cedar -**Comprehensive Environmental Data and Reporting System
- **GIS Integrator** -Geographic Information Systems
- **Cardinal** (useful for travel, payroll, etc.)
- **Culvert-Soft –** Culvert Calculations for Checking overtopping Roadway

Research/Internship Inner Mongolia, China May-Aug 2018

- Water and Wind Erosion Research, Steppe Grassland

Activities

American Society of Civil Engineers (ASCE) Aug 2014- May 2018

ASCE Concrete Canoe Team Aug 2014- May 2018

- 2017-18 Project Manager, 2016-17 Construction Manager
- Designing, Building, and Competing of a Concrete Canoe
- Attending Virginia's ASCE Conference

Chi Epsilon Civil Engineering Honor Society Dec 2016- May 2018

- Treasurer & Secretary